Biomedical Signal Processing and Control 99 (2025) 106889

Contents lists available at ScienceDirect

Biomedical Signal Processing and Control

journal homepage: www.elsevier.com/locate/bspc

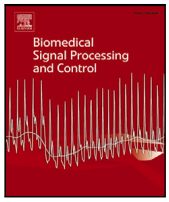

SPECTER - The Signal sPECtrum Tensor decomposition and Eye blink Removal algorithm

Zuzana Rošťáková [a,*], Roman Rosipal [a,b], Leonardo Jose Trejo [b]

[a] Institute of Measurement Science, Slovak Academy of Sciences, Dúbravská cesta 9, Bratislava, 841 04, Slovakia
[b] Pacific Development and Technology, LLC, 408 Hill Street, Capitola, 95010, CA, USA

ARTICLE INFO

Keywords:
Eye blink removal
Tensor decomposition
Electroencephalogram

ABSTRACT

Objective: Removing ocular artefacts due to eye blinks and movement is an essential preprocessing step in an electroencephalogram (EEG) analysis. Most ocular correction algorithms are based on linear regression or blind source separation algorithms such as independent component analysis (ICA). Despite their popularity and wide applicability, they also show several areas for improvement such as requiring separate electrooculogram (EOG) signals or distortions of the EEG signals due to overcorrections.
Methods: Preliminary studies have shown tensor decomposition as a promising alternative to the ocular artifact correction problem. To extend this line of research, we propose the SPECTER algorithm, which is the Signal sPECtrum Tensor decomposition and Eye blink Removal algorithm.
Results: On real data, the algorithm provided comparable or superior performance to ICA- or regression-based artifact correction methods and outperformed existing tensor-based approaches for eye blink removal. SPECTER also leads to accurate results when traditional eye blink correction methods distort EEG signal.
Conclusion: In this study, we do not aim to compete with ICA, regression-based, or other eye blink removal approaches, whose good performance has been proven in the literature. We propose the SPECTER algorithm as an alternative and flexible method in situations where traditional algorithms may fail or identification of the latent eye blink tensor components is preferred while inspecting EEG data.
Significance: SPECTER's functionality extends beyond eye blink removal, allowing it to remove a variety of other artifacts, or even more specific EEG rhythms or other EEG elements.

Introduction

The human electroencephalogram (EEG) recordings may contain artifacts due to eye movements or blinking. Omitting time segments with eye blink artifacts, manually or automatically, usually leads to an unnecessary loss of useful information. Filtering out unwanted eye movement or blinking signals while retaining the important features of brain potentials within the EEG signal should be superior to discarding segments of recordings. However, it is a difficult and not yet optimally solved task. A wide range of eye blink correction methods has been described in the literature. Based on the type of approach, they can be divided into two categories - regression-based methods and techniques that use component (latent space) decomposition, also referred to as blind source separation.

The regression-based methods [1,2] assume that the scalp EEG consists of a linear combination of ocular and brain potentials. Consequently, subtracting an appropriate multiple of one or more electrooculogram (EOG) channels from an EEG channel results in an eye blink-free EEG signal. The transmission coefficients between EOG and EEG channels are estimated by regression analysis.

However, regression-based methods only apply when the EOG measurement is present or can be properly estimated from frontal EEG, which is often not optimal. Moreover, the brain potentials can also contaminate EOG recordings. Consequently, subtracting an EOG multiple from the EEG signal may remove important information by reducing neural activities common to the frontal or reference electrodes [3]. This problem was shown to be partially solved by applying an appropriate EOG filter [4].

The second set of ocular correction methods applies when EOG measurement is missing. The EEG signal is decomposed into latent (unobserved) components that are subsequently checked for blink-related properties. The "cleaned" EEG signal can be reconstructed in two ways - either as a linear combination of the remaining non-blink components or by removing the blink components from the original data [5,6].

* Corresponding author.
E-mail address: zuzana.rostakova@savba.sk (Z. Rošťáková).

https://doi.org/10.1016/j.bspc.2024.106889
Received 22 August 2023; Received in revised form 4 July 2024; Accepted 7 September 2024
Available online 16 September 2024

In the time domain, the most popular methods for this purpose are principal component analysis (PCA) [6,7] and independent component analysis (ICA) [5,8,9]. In both cases, the EEG signal (*time points* × *electrodes*) is decomposed into a set of latent components represented by their temporal and spatial characteristics (signatures). Frequency characteristics are obtained by the spectral analysis of the component's temporal signature.

The limitation of PCA lies in the assumption of the components' orthogonality which is rarely satisfied in the real data case [5]. This assumption is replaced by component independence in ICA. The ICA-based ocular correction algorithms are widely used in the EEG literature [10]. However, several authors report problems with distortion of the EEG signal when a version of ICA is applied to eye blink-contaminated simulated or real EEG data [4]. In some cases, the spectrum of ICA-corrected EEG signal may lie above the original signal spectrum, implying the presence of artificial contamination in ICA-corrected EEG.

The multichannel EEG signal can also be represented as an N-way array or tensor, for example, in the time-space-frequency domain. Tensor decomposition methods can successfully analyze the latent structure of EEG tensor [11–15]. In our previous studies [16,17], the parallel factor analysis (PARAFAC) [18,19] and the Tucker model [20] successfully detected subject-specific narrow-band EEG oscillatory rhythms and were shown to overcome traditional matrix decomposition approaches [21]. We argue that tensor decomposition methods are also applicable to ocular correction problems.

A short remark about artifact detection using tensor decomposition, especially PARAFAC, can be found in [11]. Acar et al. [22] used the Tucker model to detect and remove eye blinks and other artifacts from EEG tensor data. However, the "cleaned" tensor was not transformed back to an EEG signal but formed an input to another tensor decomposition step to detect the seizure origin of epilepsy. The PARAFAC model was applied to a fourth-order EEG tensor also in [23], and the spatial signatures of eye blink-related components were used as a template in the spatially constrained blind signal separation algorithm.

The most similar procedure to ours is described in [24]. In this case, the EEG tensor is constructed by the continuous wavelet transform (CWT), and the Tucker model is applied. Then, the temporal signatures related to eye blink artifacts are detected and set to zero. Finally, the reconstructed "cleaned" tensor is transformed back to the time-space domain using the inverse wavelet transform (iCWT). This algorithm will be denoted as CWT-Tucker ocular correction (CWT-Tuc-OC) in the following text.

In this study, we propose to combine artifact detection by tensor decomposition and signal reconstruction from the amplitude spectrum described in [25]. Therefore, it is called a SPECTER - the Signal sPECtrum Tensor decomposition and Eye blink Removal. In contrast to [24], we focus on the amplitude spectrum of windowed EEG signal in the tensor construction step instead of CWT. As we will show later, this step significantly simplifies computational issues which may occur when CWT is applied. Moreover, the latent components extracted from the amplitude spectrum allow a more natural neurophysiological interpretation than CWT-Tuc-OC.

In the paper, the results of SPECTER are compared with the widely used regression-based Gratton-Coles & Donchin (GCD) algorithm [2] and ICA-based ocular correction method. The CWT-Tuc-OC algorithm provided inferior results and is described in Appendix B.

Because detecting and evaluating the effect of EOG artifacts on the EEG recordings is highly subjective, we do not aim to compete with the existing popular ocular correction algorithms. The proposed algorithm is an alternative approach where ICA or other traditional methods do not work well or lead to distortion of the EEG signal.

The article is organized as follows: Section 1 starts with the definition of notations, a description of tensor decomposition methods, an approach for tensor component removal, and the inverse transformation of the spectrum to signal. The proposed algorithm is described in Section 2. Section 3 introduces two real EEG datasets contaminated with eye blink artifacts which are used in Section 4 to demonstrate the performance of the SPECTER algorithm in comparison to conventional methods. The advantages and disadvantages of the methods are discussed, and the conclusions are stated in Section 5.

1. Methods

1.1. Basic notation

In the following text, an underlined uppercase letter $\underline{X} \in \mathbb{R}^{J_1 \times J_2 \times \cdots \times J_N}$ represents an N-way tensor ($N \geq 3$). Matrices are denoted by uppercase letters $X \in \mathbb{R}^{J \times K}$, vectors by bold lowercase letters $\mathbf{x} \in \mathbb{R}^J$ and scalars by lowercase letters $x \in \mathbb{R}$. An $m \times m$ identity matrix is denoted by $\mathbb{I}_m$, and $\mathbb{O}_{m \times n}$ represent an $m \times n$ zero matrix. The notation and definition of the Kronecker ($\otimes$) and outer product ($\circ$) follows the nomenclature used in [26, Section 1.4.5].

The Frobenius norm of a tensor $\underline{X} \in \mathbb{R}^{J_1 \times J_2 \times \cdots \times J_N}$ is defined by the following formula

$$\|\underline{X}\|_{Fro} = \sqrt{\sum_{j_1=1}^{J_1} \cdots \sum_{j_N=1}^{J_N} x_{j_1 \ldots j_N}^2}.$$

A one-dimensional tensor fragment, which we obtain by fixing all indices except one, will be denoted as a tensor fiber. Fixing all indices except two results into a tensor slice (two-dimensional tensor fragment) [26].

A tensor unfolding or matricization describes the operation that turns a tensor into a matrix. In this study we focus only on the mode-n unfolding as described in [26], where the mode-n fibers of a tensor $\underline{X} \in \mathbb{R}^{J_1 \times J_2 \times \cdots \times J_N}$ are arranged as columns of matrix $X_{(n)} \in \mathbb{R}^{J_n \times \prod_{k \neq n} J_k}$.

1.2. Tensor decomposition methods

The parallel factor analysis (PARAFAC) [18,19] and the Tucker model [20] represent two widely used approaches for tensor decomposition. In both models, an N-way tensor $\underline{X} \in \mathbb{R}^{J_1 \times J_2 \times \cdots \times J_N}$ is decomposed into a core (mixing) tensor

$$\underline{G} \in \mathbb{R}^{K_1 \times K_2 \times \cdots \times K_N}$$

and N component matrices

$$A^{(n)} = \left(\mathbf{a}_1^{(n)}, \mathbf{a}_2^{(n)}, \ldots, \mathbf{a}_{K_n}^{(n)}\right) \in \mathbb{R}^{J_n \times K_n}, n = 1, \ldots N,$$

where $K_n, n = 1, \ldots, N$ is the number of latent components in the nth mode.

The Tucker model follows the formula

$$\begin{aligned}
\underline{X} &= \underline{G} \times_1 A^{(1)} \times_2 A^{(2)} \times_3 \ldots \times_N A^{(N)} + \underline{E}, \\
\underline{X} &= \sum_{k_1=1}^{K_1} \sum_{k_2=1}^{K_2} \cdots \sum_{k_N=1}^{K_N} g_{k_1 k_2 \ldots k_N} \mathbf{a}_{k_1}^{(1)} \circ \mathbf{a}_{k_2}^{(2)} \circ \ldots \circ \mathbf{a}_{k_N}^{(N)} + \underline{E}, \\
x_{j_1 j_2 \ldots j_N} &= \sum_{k_1=1}^{K_1} \sum_{k_2=1}^{K_2} \cdots \sum_{k_N=1}^{K_N} g_{k_1 k_2 \ldots k_N} a_{j_1 k_1}^{(1)} a_{j_2 k_2}^{(2)} \ldots a_{j_N k_N}^{(N)} + e_{j_1 j_2 \ldots j_N}, \qquad (1)
\end{aligned}$$

where an N-way tensor $\underline{E} \in \mathbb{R}^{J_1 \times J_2 \times \cdots \times J_N}$ represents an error term. The tensor-matrix multiplication in the nth mode is denoted by $\times_n, n = 1, \ldots, N$ [26].

On the other hand, the PARAFAC model assumes the same number of components $F = K_1 = \cdots = K_N$ in all modes and a super-diagonal structure of $\underline{G}$. Consequently, the PARAFAC model formula simplifies to

$$\begin{aligned}
\underline{X} &= \underline{G} \times_1 A^{(1)} \times_2 A^{(2)} \times_3 \ldots \times_N A^{(N)} + \underline{E}, \\
\underline{X} &= \sum_{f=1}^{F} g_{ff \ldots f} \mathbf{a}_f^{(1)} \circ \mathbf{a}_f^{(2)} \circ \ldots \circ \mathbf{a}_f^{(N)} + \underline{E},
\end{aligned}$$

$$x_{j_1 j_2 \dots j_N} = \sum_{f=1}^{F} g_{ff\dots f} a^{(1)}_{j_1 f} a^{(2)}_{j_2 f} \dots a^{(N)}_{j_N f} + e_{j_1 j_2 \dots j_N}. \quad (2)$$

To avoid multiplication ambiguities, component matrices $A^{(n)}, n = 1, \dots, N$ in both models are assumed to have normalized columns [26] and are denoted as signatures in the following text [11,17,21]. Interpretation and stability of the decomposition can be improved by constraining the component matrices, for example, to orthogonal [22], nonnegative [11,14,17], uni- or bi-modal columns [21,27].

Following [11], we consider only the PARAFAC model for the eye blink detection, mainly due to the straightforward interpretability of the solution. This contrasts with [22,24], where the Tucker model is preferred. Nevertheless, the whole analysis presented in this study was repeated with the more flexible Tucker model, but we did not observe any significant improvement in results compared to PARAFAC.

1.3. Removing components in PARAFAC

In the literature, three approaches for the eye blink removal from the data tensor $\underline{X}$ are described - component zeroing, component subtraction, and projection to the nullspace of space spanned by selected components [22,24].

However, only the component subtraction was observed to be appropriate within the SPECTER algorithm. A description of the other two methods for both PARAFAC and Tucker model can be found in Appendix A. Their usability and performance when applied in the SPECTER approach are discussed in Appendix A.1.

Let us assume the PARAFAC model (2), the corresponding estimated component matrices $A^{(1)}, \dots, A^{(N)}$, and the super-diagonal core tensor $\underline{G}$. Let S_{rem} be an index set of artifact components to remove. Then, the component subtraction step is defined as

$$\underline{X}_{rem} = \underline{X} - \sum_{f \in S_{rem}} g_{f\dots f} \mathbf{a}^{(1)}_f \circ \dots \circ \mathbf{a}^{(N)}_f = \sum_{f \notin S_{rem}} g_{f\dots f} \mathbf{a}^{(1)}_f \circ \dots \circ \mathbf{a}^{(N)}_f + \underline{E}.$$

1.4. Spectrum to signal transformation

The amplitude spectrum can be directly computed from raw EEG, for example, by the Fast Fourier transform. However, the inverse procedure – from spectrum to signal – is more complex since the phase information is usually missing, and only the amplitude spectrum is available.

For a given amplitude spectrum, the Griffin-Lim algorithm (GLA) [28] aims to find a complex-valued spectrogram C satisfying two conditions - absolute values of C coincide with the given amplitude spectrum and C belongs to the image of the short-time Fourier transform (STFT) with a given time window (consistency condition). The raw signal is then reconstructed from the estimated spectrogram C by the inverse STFT.

However, the original algorithm was shown to require too many iterations or may get stuck in a local optimum, resulting in phase recovery of low quality [25]. Therefore, several modifications of the original GLA can be found in the literature [29–31]. In this study, we applied the Griffin-Lim like phase recovery via the alternating direction method of multipliers (ADMMGLA) [25], which produced the most stable and satisfying results in our case.

Moreover, Masuyama, Yatabe, and Oikawa [25] claim that in some specific situations, it can be rather complicated to find a spectrogram satisfying both conditions, or such a spectrogram does not have to exist. Because the strict equality between a given amplitude spectrum and the absolute value of the spectrogram is always required, they recommend relaxing the consistency condition [25, Section III B]. The order of relaxation is controlled by the $\rho \geq 0$ parameter, with $\rho = 0$ representing the situation with both conditions satisfied.

2. SPECTER algorithm

The SPECTER algorithm combines the procedures mentioned in the previous section - tensor decomposition of the signal spectrum, artifact removal by component subtraction, and spectrum-to-signal transformation by ADMMGLA. To make the algorithm more readable, we summarized it into several steps, and the graphical schema is depicted in Fig. 1.

(1) Signal spectrum and tensor construction. The EEG signal is divided into overlapping time windows in the first step. In this study, we applied 0.5-second time windows with a 80% of overlap (0.4 s). To select a time window of appropriate length, we ran the SPECTER's algorithm without eye blink removal step for various time windows (0.5 s, 1 s, 1.5 s, 1.75 s, 2 s, 2.5 s, 3 s). Then, Pearson's correlation coefficient was computed between the original (eye-blink corrupted) and reconstructed signal. The resulting correlations were generally high (>0.95) but slightly decreased with the increasing window length. However, we observed short intervals with signal distortions in the reconstructed signal when the window length exceeds 1.75 s. Therefore we decided to select a 0.5-second time window for this analysis.

For each time window and each electrode, the amplitude spectrum of the EEG signal is computed by the Fast Fourier transform (FFT). The obtained spectrum values are arranged into the tensor $\underline{X} \in \mathbb{R}_{+}^{J_1 \times J_2 \times J_3}$, where J_1 is the number of time windows, J_2 is the number of electrodes, and J_3 is the number of frequencies. The tensor $\underline{X}$ is nonnegative because the amplitude spectrum does not include negative values.

(1a) $\log_{10}$ transformation. After the tensor construction, it is possible to apply tensor decomposition followed by component removal directly. However, neither component subtraction nor component zeroing or projection to the nullspace (Appendix A) guarantees the nonnegativity of the resulting tensor $\underline{X}_{rem}$. Negative values cannot represent the spectrum of any signal, and therefore, physiological interpretation would be missed. Moreover, the ADMMGLA method requires only nonnegative values representing the amplitude spectrum of a signal. Unfortunately, setting the negative values in $\underline{X}_{rem}$ to zeros would lead to rapid distortions in the reconstructed signal.

Therefore, in our algorithm's intermediate step, we use the log_{10} transform of $\underline{X}$ before the tensor decomposition. The transformed tensor $\underline{X}^{\star} = log_{10}(\underline{X}) \in \mathbb{R}^{J_1 \times J_2 \times J_3}$ is not nonnegative any more. But what is more important, the inverse transformation (the power of 10) after the tensor decomposition and component subtraction guarantees $\underline{X}_{rem}$ to be nonnegative.

(2) Tensor decomposition and dominant signature pattern detection. Following [32], tensor $\underline{X}^{\star}$ is centered in the first (temporal) mode ($\underline{X}^{\star}_{centr}$) and the PARAFAC model with nonnegativity constraints in the temporal, spatial and frequency modes is applied [16,17,21].

The appropriate number of components in PARAFAC is usually selected by a priori information or using a preferred component number selection method. However, our previous study [33] showed that many component number selection methods must be revised for EEG data.

The cumulative component clustering procedure (*tripleC*) [33] was successfully applied in our previous study focusing on EEG tensor decomposition [17] and was shown to overcome the majority of component number selection methods [33]. In *tripleC*, the results of PARAFAC models with 1 to F_{max} components are merged into one set and assigned into clusters by the non-parametric density-based clustering (DBscan) [34]. The DBscan algorithm has two parameters [34]: (i) the number of neighbors, which was set to two to avoid potential outlier components, and (ii) the diameter of a component neighborhood was chosen between 0.6 and 1 for the majority of subjects in both datasets described in Section 3. The number of clusters varied between three and ten mirroring the data complexity and the number of different oscillations and artefacts.

General components are then characterized by averaged normalized temporal, spatial, and frequency signatures of dominant clusters and

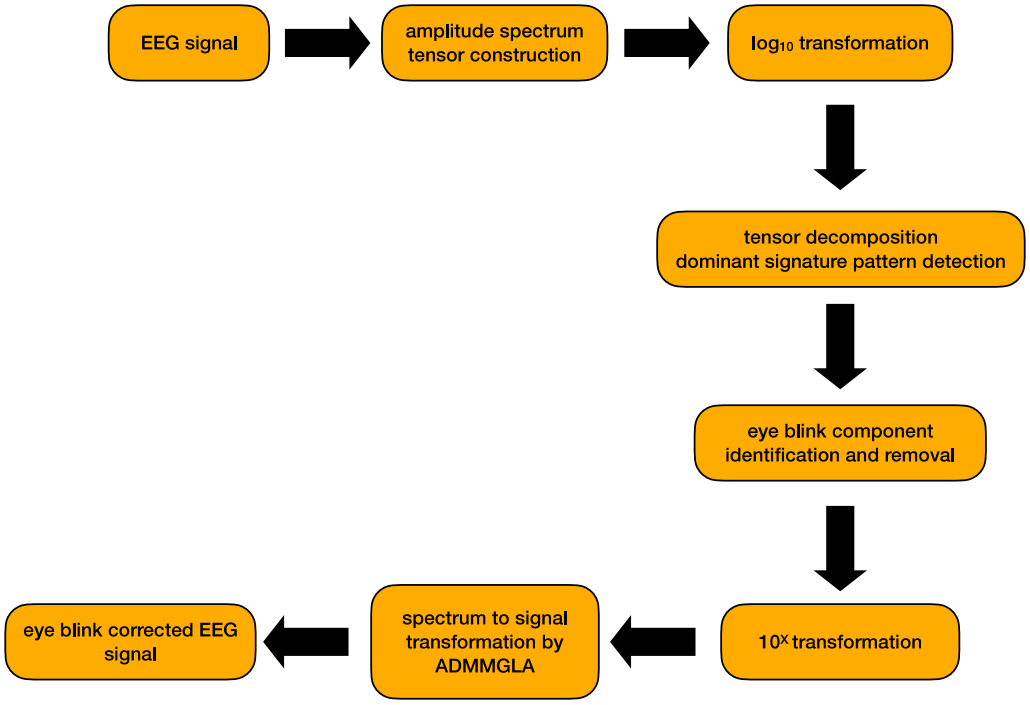

Fig. 1. Graphical schema of SPECTER - the Signal sPECtrum Tensor decomposition and Eye blink Removal method.

form general component matrices $A_c^{(1)}$ (temporal), $A_c^{(2)}$ (spatial) and $A_c^{(3)}$ (frequency).

In a single PARAFAC model with a fixed number of components, each component follows its weight represented by the corresponding diagonal element of $\underline{G}$. However, this information is missing after the *tripleC* procedure. Nevertheless, $\underline{G}_c$ can be estimated by the least squares criterion

$$\underline{G}_c \in \operatorname{argmin}_{\underline{H}\in\mathbb{R}^{F\times\cdots\times F}} \|\underline{X}^{\star}_{centr} - \underline{H} \times_1 A_c^{(1)} \times_2 A_c^{(2)} \times_3 A_c^{(3)}\|_F, \tag{3}$$

under the super-diagonality constraints.

(3) Eye blink identification and removal. General components representing eye blink artifacts are visually selected by an expert analyst and subtracted from tensor $\underline{X}^{\star}$ as described in Section 1.3.

The visual selection criteria include:

(i) presence of short intervals of higher amplitude in time scores (TS),
(ii) visual overlap of time scores and EEG signal from frontal electrodes like Fp1, Fp2, or Fpz (or AF3, AF4 and AFz if the signal from the previously mentioned electrodes is unavailable),
(iii) spatial signatures with higher weights for frontal electrodes,
(iv) frequency signatures representing either oscillatory activity over low frequencies up to 4 Hz or distributed over a set of frequencies without one clear peak over a single frequency.

However, some users may prefer an automatic component selection. Altogether, most algorithms used for an automatic component selection when using ICA for eye blink removal may also be applicable in SPECTER. In this study, we compared the results of the eye blink component visual selection with the following approaches:

- The ADJUST algorithm [35] was initially developed for automatic eye blink selection of ICA components. ADJUST selects eye blink latent components by inspecting their spatial and temporal features. We used the ADJUST plugin within the EEGLAB software [36].
- Spearman's correlation coefficient between component time scores and EEG from frontal electrodes Fp1 and Fp2 (or AF3 and AF4 if the signal from the previously mentioned electrodes is unavailable) [5] above a predefined threshold T_ρ. In this study, we considered $T_\rho = 0.4$.
- Kurtosis of component TS above a predefined threshold, as described in [37]. Highly positive kurtosis indicates a peaky distribution of TS values, which is typical for eye blink-related components [37].

(3a) $10^{\mathbf{X}}$ transformation:. Tensor $\underline{X}^{\star}_{rem}$ is transformed back into the nonnegative form by the following formula

$$\underline{X}_{rem} = 10^{\underline{X}^{\star}_{rem}},$$

where the power of 10 to a tensor is understood in an element-wise way.

(4) Spectrum-to-signal transformation. Finally, ADMMGLA with relaxed consistency condition is applied to transform the cleared spectrum back into the time domain. In the study, we set the ρ parameter to 0.1. The value was determined by optimizing the correlation between the original and reconstructed EEG signal using a subset of EEG recordings.

2.1. Opposite sign and slight time shift problems

Due to the lack of phase spectrum information, the original and reconstructed signal can follow approximately the same values but with the opposite sign over subintervals (Fig. 2, left column). These subintervals were observed to be consistent with the 100 ms step size used to construct the signal spectrum[1] in Section 2.

To mitigate this problem, we propose a simple heuristics. For each 100 ms time window, we computed Spearman's correlation coefficient ρ between the original and reconstructed signal. If ρ was negative, the reconstructed signal was multiplied by -1 within this time window.

[1] The EEG signal was divided into 0.5-second time windows with an 80% overlap (0.4 s). Consequently, the step size of the sliding window was 100 ms (0.1 s).

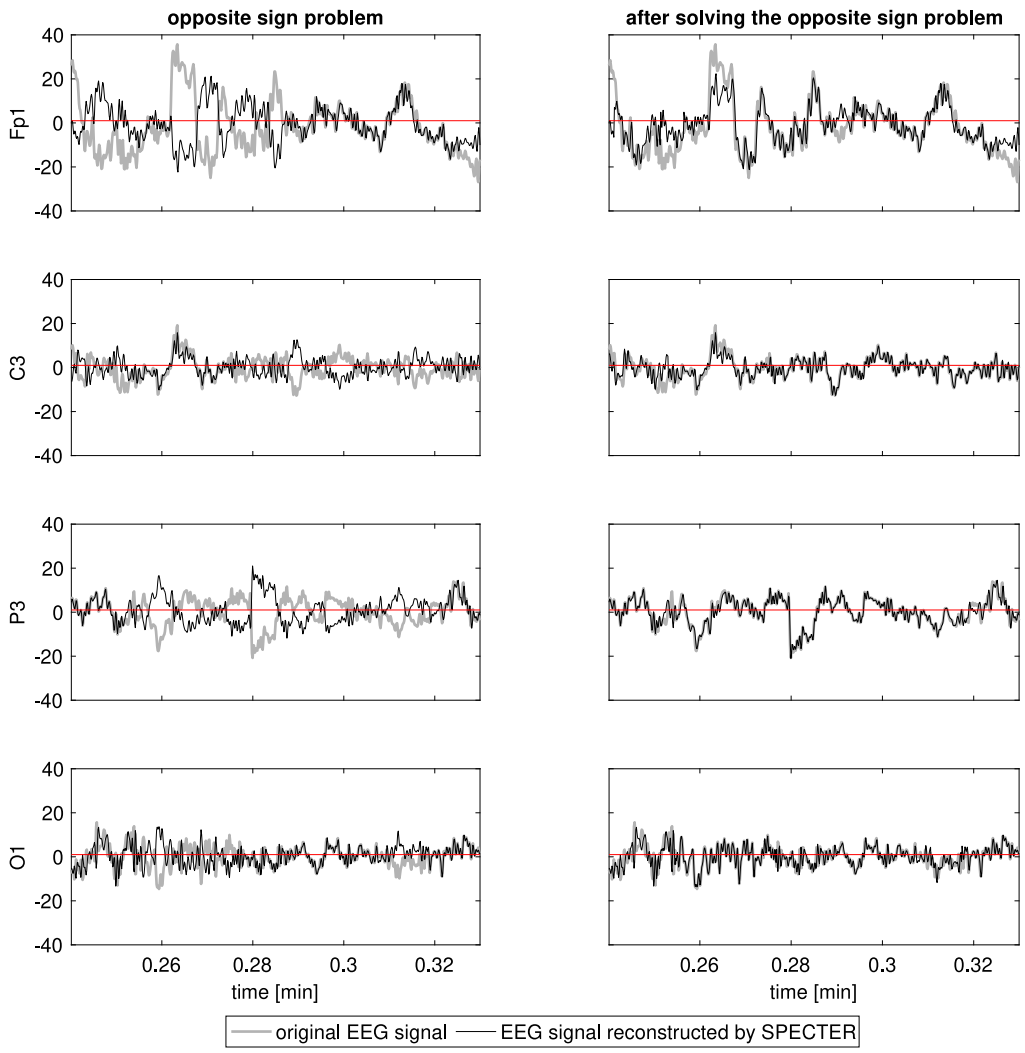

Fig. 2. Comparison of the original EEG signal (gray) and the reconstructed signal by SPECTER (black) from four left hemisphere electrodes before (left column) and after (right column) applying simple heuristics for solving the opposite sign problem. The red line depicts a zero line. In the left column, a better match would be achieved by changing the sign of the reconstructed signal values over time subintervals (right column).

If ρ was positive but insignificant, we computed the distance between the original EEG signal and the reconstructed signal multiplied by 1 or -1 and chose a version leading to a lower distance. The heuristics successfully corrected the majority of sign differences between signals (Fig. 2, right column). Nevertheless, a method for robust mitigation of the sign problem in the reconstructed signal is still needed.

The second problem is depicted in Fig. 3. Due to signal windowing within the SPECTER algorithm, the reconstructed EEG signal was observed to be shifted either one point to the left (Fig. 3, left, black color) or one point to the right (Fig. 3, right, black color) in comparison to the original EEG signal (Fig. 3, gray color) over some short subintervals ($\approx$100 ms). Due to slight time shifts in both directions, it was impossible to shift the whole reconstructed EEG signal, either several time points to the left or to the right. Consequently, evaluating the SPECTER's performance using a correlation coefficient with the original EEG signal or other statistical measures sensitive to this shift is inappropriate; SPECTER would produce numerically inferior results despite its superior eye blink removal performance.

The problem can be solved using the dynamic time warping algorithm (DTW) [38].[2] DTW tries to find an optimal warping path between two time series to minimize the Euclidean distance between them. Since the shifts between the raw EEG and reconstructed signal by SPECTER were observed to be one point in the majority of cases and at most three time points, it is possible to restrict the warping path to be at most three points of the straight line fit (original time).

Finally, a solution to both these problems is to detect short intervals around each eye blink in the original EEG signal and to replace these selected intervals with corresponding reconstructed signal values. Consequently, the EEG signal remains unchanged over the non-blink intervals. For example, the time intervals with eye blinks can be detected by an automatic thresholding method [40] originally proposed for spike detection in neural data or another preferred eye blink detection method.

The opposite sign and slight time shift problems are only present when analyzing the reconstructed EEG signal in the time domain. But what is more important, they do not affect the reconstructed signal spectrum. Consequently, if we are interested in the eye blink-free EEG signal spectrum rather than its analysis in the time domain, both problems can be safely ignored.

3. Data

Two datasets with corrupted eye blink EEG signals were used to demonstrate the SPECTER method's ability to remove eye blinks.

[2] For this purpose, the MATLAB routine *dtw* can be used [39].

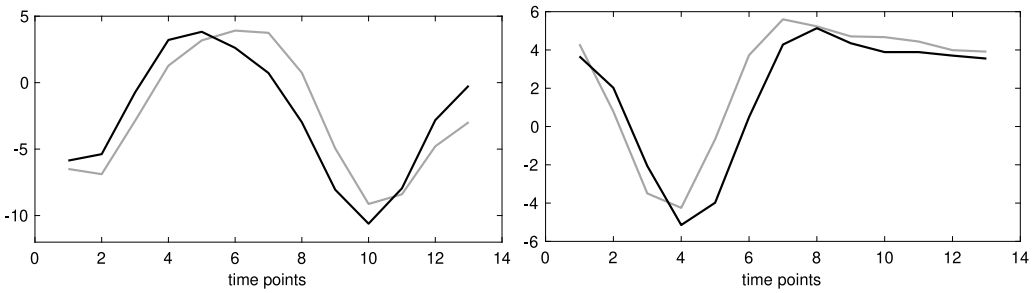

Fig. 3. Comparison of the original EEG signal (gray) and signal reconstructed by SPECTER (black) over two short time intervals consisting of 13 time points (≈100 ms).

Table 1
The eyes open EEG measurements duration (in seconds) for three subjects before (SubX_pre), during (SubX_med), and after meditation (SubX_post).

	_pre [s]	_med [s]			_post [s]
Sub1	90	393	312	301	68
Sub2	60	678			59
Sub3	61	93			65

3.1. Dataset 1

The first dataset consists of 11 EEG measurements from three healthy adult male volunteers seated comfortably with eyes open [41]. The subjects received an explanation of the purpose and procedures of the study, which they fully understood, and gave written informed consent to participate. Subjects were asked to relax in a peaceful meditative state. For each subject, approximately one minute of EEG measurement of relaxed eyes open condition before (SubX_pre) and after meditation (SubX_post) was available. Moreover, Subject 1 followed three measurements of the eyes open meditation (Sub1_med1, Sub1_med2, Sub1_med3), and Subjects 2 and 3 had one measurement (Sub2_med, Sub3_med). The time duration of each EEG measurement is described in Table 1.

The EEG signal was measured by a 64-channel BioSemi EEG recording system (Biosemi B.V.) with a 512 Hz sampling rate [21,41]. In addition, horizontal and vertical EOG were recorded. In this study, 19 EEG electrodes - Fp1, F3, F7, C3, T7, P3, P7, O1, Pz, Fp2, Fz, F4, F8, Cz, C4, T8, P4, P8 and O2, were used. In the preprocessing step, the EEG data were downsampled to 128 Hz, re-referenced to linked ears and filtered by using a high-pass 8th order Butterworth filter with a cut-off frequency of 0.5 Hz in the BrainVision Analyser 2 (BVA2) software [42]. Then, a low-pass filter with a cut-off frequency of 30 Hz was applied using the MATLAB routine *filtfilt*. An example of the EEG signal from eight left-hemisphere electrodes is depicted in Fig. 4. Fig. 5 shows the whole VEOG signal of Sub1_med2, two short time intervals of EOG with one blink, and the corresponding amplitude spectra.

In BVA2, both the VEOG and HEOG channels were selected as input parameters for GCD, and the eye blink detection and corrections were run automatically.

Regarding ICA, the VEOG channel was used as the blink marker channel and scanned for blinks by the mean slope algorithm in the first step. Afterward, the FastICA algorithm was applied to the entire EEG recording. The number of ICA steps and convergence bounds were set to 150 and 10^{-7}, respectively. A proportion of variance shared between the VEOG channel and ICA components was then used to identify the ICA components related to VEOG activity. In this step, BVA2 focuses only on time intervals with blink markers [43]. If the proportion of variance was above 30%, the component was labeled as ocular and removed from the data together with other ocular components in the next step.

3.2. Dataset 2

The OSF EEG eye artifact dataset is a public dataset of eye blink corrupted EEG data, available at https://osf.io/2qgrd/. The whole dataset consists of EEG data from five studies. We focused on data from study01, study02, study03, and study04 consisting of EEG measurements from 5, 14 (one subject from study02 was removed due to an insufficient number of eye blinks), 10, and 15 subjects, respectively. The original data description can be found in [44–48].

Together, 83 signals are available for each subject, including EEG and EOG (HEOG and VEOG) signals, EOG derivatives, artifact and other channels. To be consistent with Dataset 1, we used only the EEG signal from 19 electrodes - Fp1, F3, F7, C3, T7, P3, P7, O1, Pz, Fp2, Fz, F4, F8, Cz, C4, T8, P4, P8, and O2. However, EEG data from studies 01, 02, and 03 did not include EEG signals from electrodes Fp1 and Fp2. In these cases, we used the signal from AF3 and AF4 electrodes.

The EEG measurement for each subject was divided into two blocks. In this study, the signal from the first block was used.

The EEG signal was measured under four conditions - rest, horizontal eye movements, vertical eye movements, and eye blinks - which we call epochs in the following text. The number of epochs measured under different conditions, their repetition, and order within the first block varies across subjects. After downsampling to 100 Hz (study04) or 200 Hz (study01) and data preprocessing, each epoch took 8 s of EEG signal (800 points for sampling frequency 100 Hz and 1600 points for sampling frequency 200 Hz). Finally, the preprocessed EEG data were organized in a three-way array of the size *number of signals* × *number of samples* × *number of epochs*.

However, SPECTER cannot be run on a single epoch consisting only of eye blinks or other artefacts, because a sufficient number of intervals with both artifactual and clean EEG signals is needed. Therefore, we concatenated the EEG signal for each subject among epochs. To avoid signal discrepancies caused by concatenation, we applied moving average smoothing around the block borders (±5 time points). An example of the EEG signal from study04 is depicted in Fig. 6.

The dataset also included precomputed ICA components for each subject. The ADJUST algorithm selected the ICA eye blink components to be consistent with SPECTER. For component removal, we used the *pop_subcomp* routine in EEGLAB [36].

3.3. Method comparison

Both datasets mentioned above were selected to evaluate the SPECTER algorithm's performance in comparison to ICA and GCD.

Dataset 2 serves especially for a quantitative comparison between (i) manual selection of eye blink components and automatic component selection criteria for SPECTER and (ii) SPECTER and ICA eye blink removal algorithms. The GCD algorithm was not considered within the quantitative analysis since it directly uses information from the EOG channel, which would make the comparison unfair.

In the first step, we focused on the resting state epochs, over which the cleaned EEG signal is assumed to remain unchanged compared to

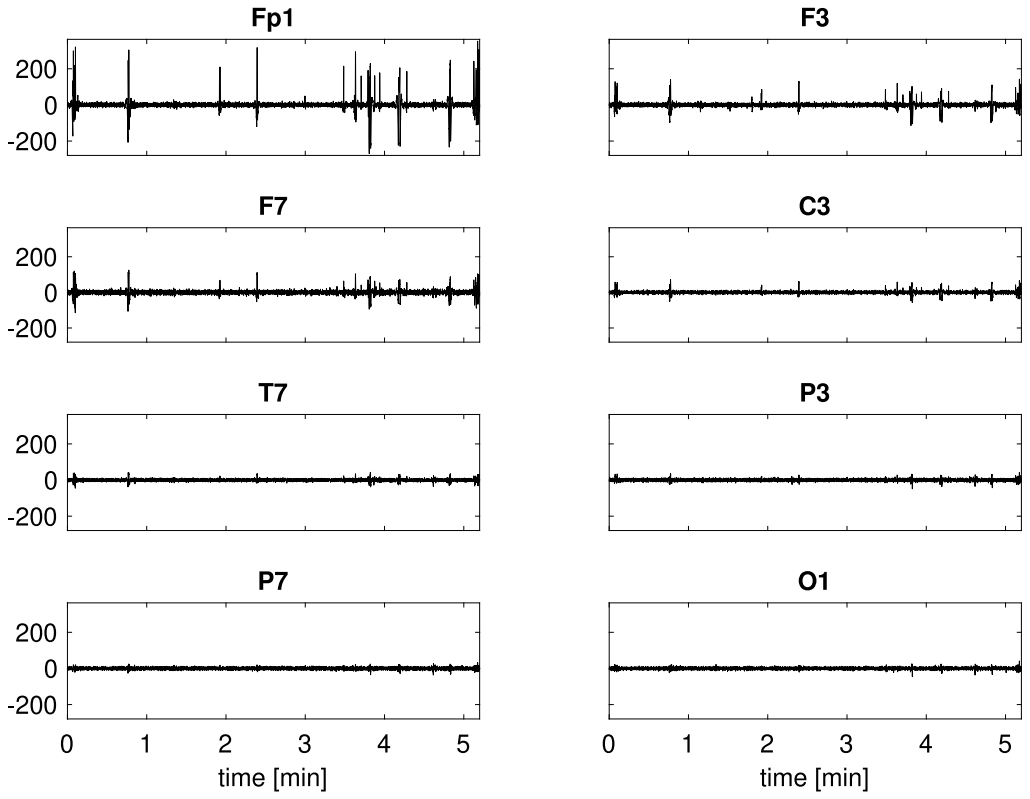

Fig. 4. Sub1_med2: An example of the EEG signal from eight left-hemisphere electrodes measured during the eyes open meditation.

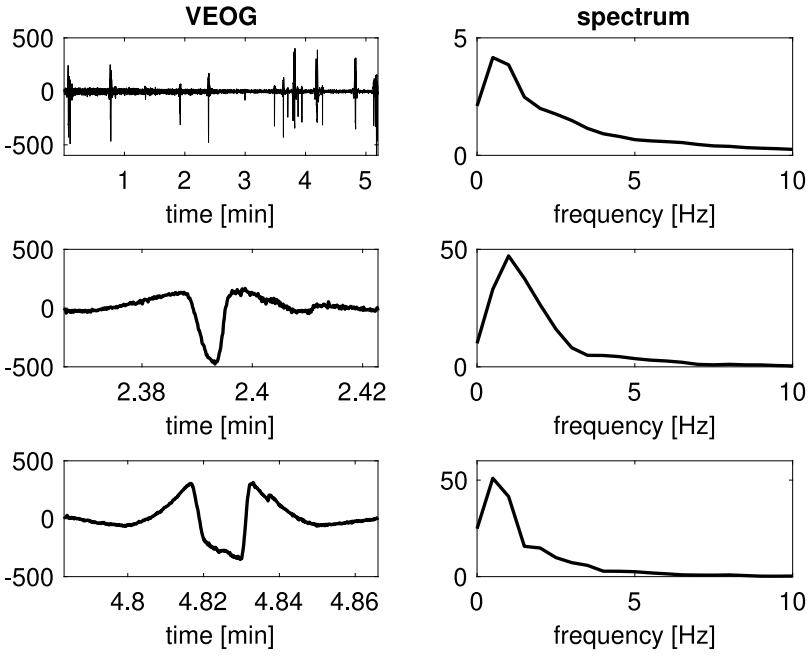

Fig. 5. Sub1_med2: An example of the amplitude spectrum (right column) of the whole VEOG signal (top, left) and two short time intervals of VEOG with one eye blink (middle and bottom, left).

its original version. As mentioned in Section 3.2, each eight-second epoch of EEG signal was labeled as rest, horizontal eye movement, vertical eye movement, or eye blinks in each subject. However, after visual inspection, we detected epochs, labeled initially as rest, including eye blinks. Therefore, for each subject, only epochs with the absolute EEG amplitude below 50 μV were considered in further analysis. Four subjects (one from study03 and three from study04) included no eye blink-free rest epochs. Consequently, the total number of subjects considered in this comparison was 40.

To compare ICA and SPECTER outcomes over the resting state epochs, we considered Spearman's correlation coefficient and the absolute difference between power spectral densities (PSD) between the original EEG signal and its versions cleaned by ICA and SPECTER. Additionally, we considered the Euclidean distance between the original

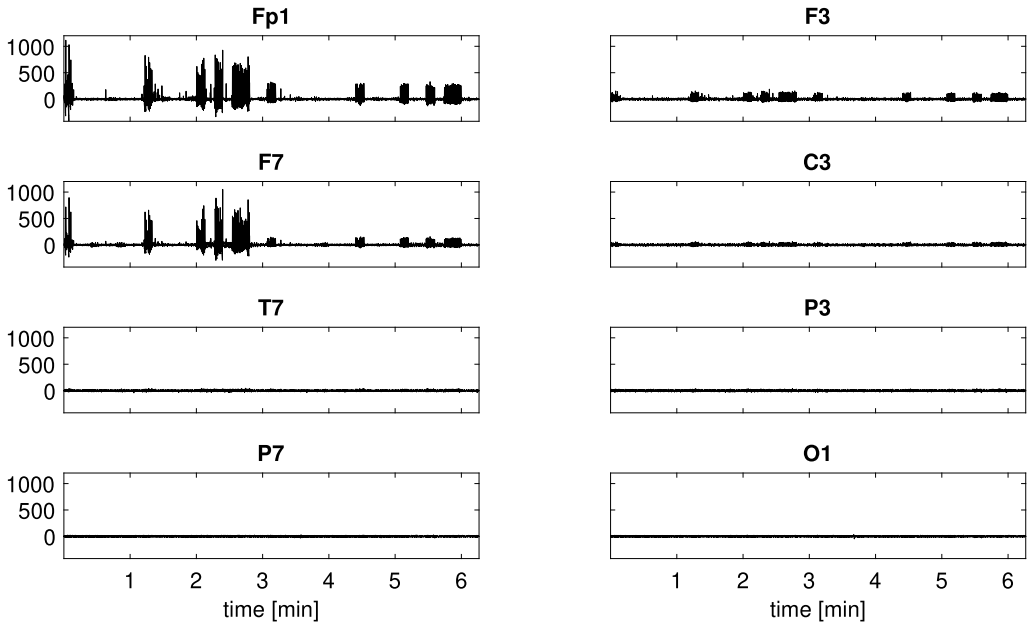

Fig. 6. Study04: An example of the concatenated EEG signal from eight left-hemisphere electrodes of one subject.

EEG signal and its version cleaned by ICA and SPECTER. However, as the conclusions mimic those based on Spearman's correlation, this measure was omitted in this study.

To avoid low correlations due to opposite sign and slight time shift problem, we applied the heuristics described in Section 2.1 and the *dtw* algorithm to the original EEG signal and the SPECTER's corrected EEG on each rest epoch and each electrode separately.

Similarly to [49,50], PSD's for the original EEG signal and its version cleaned by ICA and SPECTER were computed by the Welch's method with the two-second time windows and 1.5 s overlap in four frequency bands - delta (0.5–4 Hz), theta (4–8 Hz), alpha (8–12 Hz) and beta (12–25 Hz). EEG signals from frontal Fp1 and Fp2 electrodes (or AF3 and AF4 electrodes, if signals from Fp1 and Fp2 were unavailable) were used.

Since the true eye blink free EEG signal is unknown for Dataset 2, we took the ICA eye blink corrected EEG signal as a benchmark and computed its Spearman's correlation with the SPECTER's results over the eye blink epochs. However, if the correlations were too low, we visually inspected both ICA and SPECTER corrected EEG signal, to evaluate whether the low correlation was caused by inferior performance of SPECTER or ICA.

In Dataset 1, we focused more on the reconstructed EEG signal visual quality and performed only a qualitative comparison between SPECTER, ICA, and GCD. We focused primarily on observations in which GCD or ICA led to inferior results to demonstrate SPECTER's ability to remove eye blinks successfully in these situations. Unless otherwise stated, we focus on the results from frontal electrodes, where the effect of eye blinks is most pronounced. The reconstructed signal from other electrodes is discussed only in the case of unexpected behavior.

Finally, we also inspected the frequency spectrum to detect the potential presence of artificial frequency components added to EEG by the eye blink removal methods in both datasets.

4. Results

Section Results is divided into four parts. First part compares the visual selection of eye blink-related latent components with three automatic component selection criteria. Selected results of PARAFAC and *tripleC* in Dataset 1 are presented, and eye blink properties of estimated general time scores are discussed.

The second part quantitatively compares the quality of SPECTER's outcomes on rest and eye blink epochs in Dataset 2 with the ICA approach.

Qualitative comparison of SPECTER with the GCD algorithm [2] and ICA - both carried out by the BVA2 software [42] - is described in the third part.

The fourth part analyses a situation when the SPECTER algorithm may provide inferior results.

4.1. Eye blink component selection

4.1.1. Dataset 1

An example of PARAFAC components for Subject 1 during the second meditation session (Sub1_med2) is depicted in Fig. 7. In this case, *tripleC* found five general components.

A visual inspection of all PARAFAC components detected three eye blink-related components. In Fig. 7, components 1, 3, and 4 follow oscillatory brain activity located in the frontal brain regions. The frequency signature of selected components follows higher weights either over low frequencies ($\leq$4 Hz, component 3) or is distributed over a longer frequency interval (components 1 and 4). Both characteristics are typical for eye blinks. The corresponding time scores follow a clear spiky pattern. Moreover, short subintervals with higher TS values visually overlap with the subintervals with higher amplitude of EEG representing eye blinks at the Fp1 electrode (Fig. 7, second row).

In the second step, we applied the automatic thresholding method described in [40] to the Fp1 EEG signal with the aim to detect the time location of eye blinks. The results of the detection were manually inspected. Fig. 8 compares the general PARAFAC TS from Fig. 7 with the detected eye blink intervals. TS 1, TS 3, and TS 4 achieve higher values only over eye blink subintervals and likely indicate the eye blink presence. On the other hand, TS 2 and TS 5 achieve higher values over the whole time interval and represent other brain activity than eye blinks.

The ADJUST algorithm labeled components 1, 3, and 4 as artifactual and eye blink-related. This selection is in line with the visual inspection. The correlation between component TS and the EEG signal from the Fp1 or Fp2 electrode overcame the threshold of 0.4 only for component 3. The third selection criterion, based on the kurtosis of TS, selected only component 1 as artifactual.

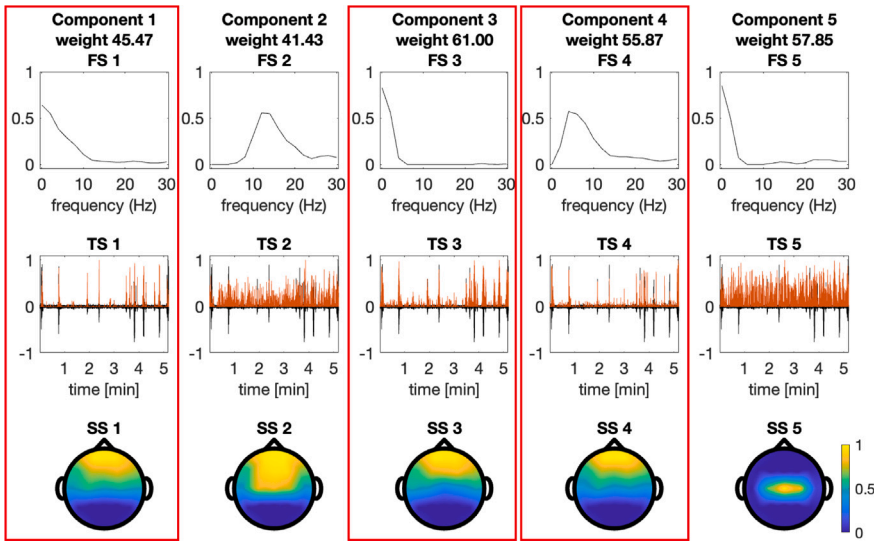

Fig. 7. Sub1_med2: PARAFAC components (columns) detected by the cluster analysis of the PARAFAC model with one to ten components - the *tripleC* algorithm. The frequency signatures (FS) are depicted in the first row together with the component weight (the corresponding diagonal elements of the core tensor $\underline{G}_c(3)$) in the title. The time scores (TS, orange) are compared with the original EEG signal from the Fp1 electrode (black) in the second row. Spatial signatures (SS) are plotted as topographic maps with the same color scale in the third row. Three components representing eye blinks selected for removal within the SPECTER algorithm are highlighted by red rectangles.

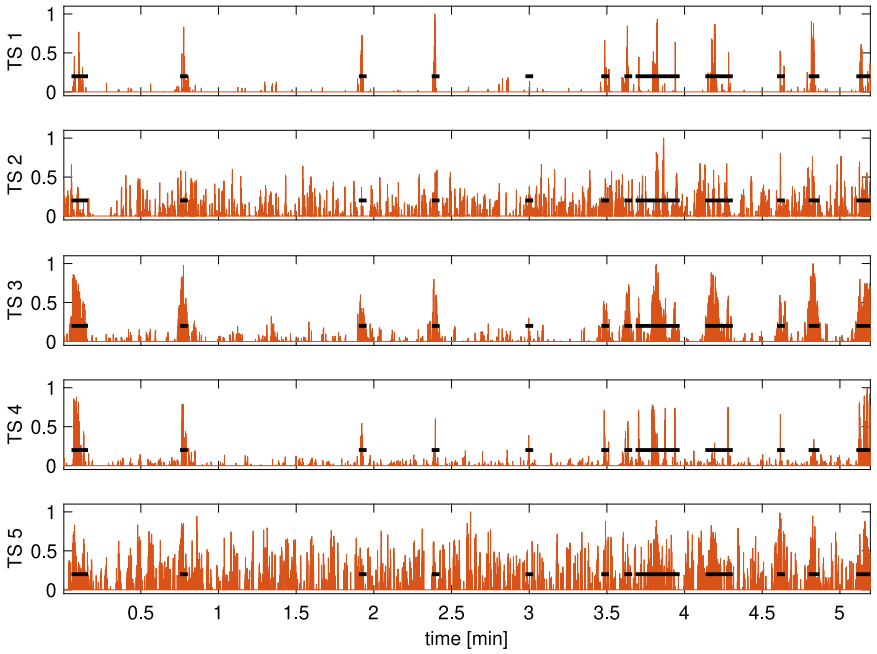

Fig. 8. Sub1_med2: Comparison of general time scores (TS, orange) from Fig. 7 and time intervals with detected eye blinks (black) at the Fp1 electrode by an automatic thresholding method [40].

Results for Subject 3 are depicted in Figs. 9 and 10. Higher amplitudes in time scores of the eye blink PARAFAC components 1 and 2 for Sub3_post data (Fig. 9) occur on the time intervals with eye blinks detected by the automatic thresholding method of the Fp1 electrode EEG signal (Fig. 10).

Components 1 and 2 were also selected using the ADJUST algorithm. The correlation with frontal electrodes exceeded the threshold of 0.4 only for component 1. The selection criterion based on kurtosis did not detect any artifactual component.

4.1.2. Dataset 2

In this subsection, we focus on a more comprehensive comparison of the eye blink component selection provided by (i) visual inspection, (ii) ADJUST algorithm, (iii) criterion based on correlation between component TS and EEG signal from frontal electrodes, and (iv) criterion based on TS kurtosis as described in Section 2. All four criteria selected one to five eye blink-related components.

For each subject, we computed the overlap between components selected by visual inspection and the other three criteria mentioned above. The following formula computed the overlap

$$O = \frac{\text{number of components selected by both methods}}{\text{number of components selected by any of the two methods}} * 100\ [\%].$$

For example, visual inspection selected components 3 and 4, and another method only selected component 4. Then, the overlap was $\frac{1}{2} * 100 = 50\%$. Suppose another method selected components 1 and 4. In that case, the number of components selected by both methods is

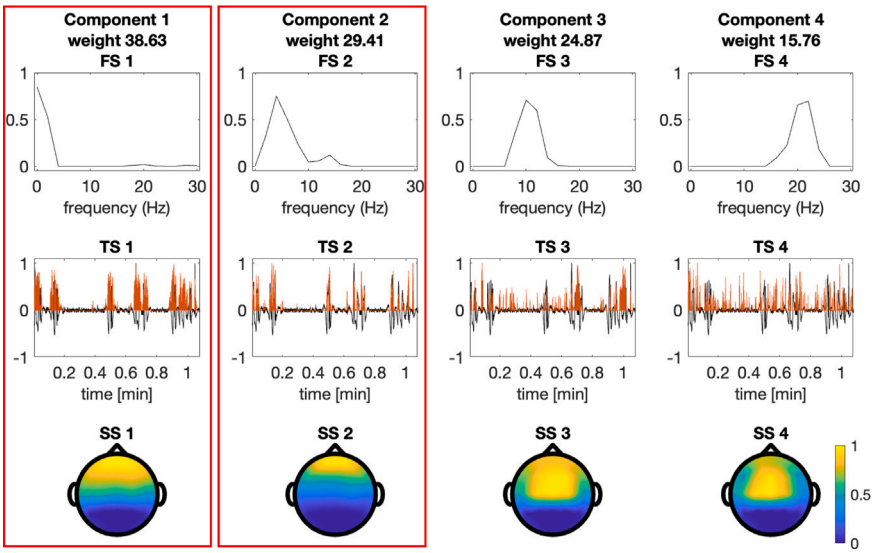

Fig. 9. Sub3_post: See Fig. 7 description.

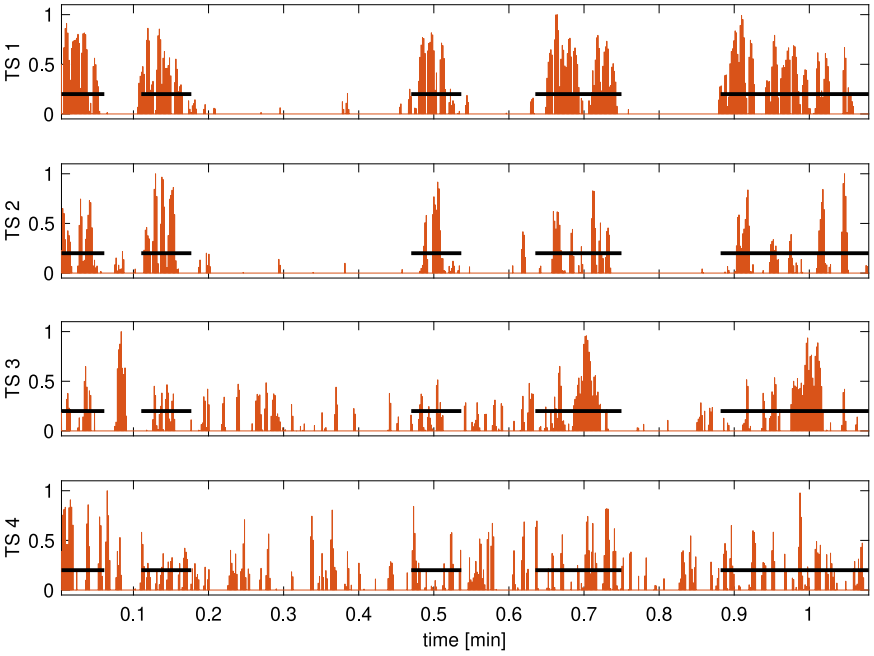

Fig. 10. Sub3_post: See Fig. 8 description.

one (component 4), and the number of unique components selected by any of the two methods is three (components 1, 3, 4). Consequently, the overlap is 33%.

The overlaps were divided into four categories - $O = 100\%$ (exact overlap), $O \in [50, 99]\,\%$, $O \in [25, 49]\,\%$, and $O < 25\%$. For each study, we computed the ratio of subjects with overlaps falling into each of the four categories. The results are depicted in Fig. 11.

In study01, visual inspection and ADJUST selected the same components in four out of five subjects (Fig. 11). The only exception was subject 03 for which the visual inspection selected components number 1 and 7 as eye blink-related (Table 2). ADJUST also selected component 1, but instead of component 7, component 2 was labeled as blink-related. Therefore, the overlap between visual inspection and ADJUST was only 33% for this subject.

Exact overlap between visual inspection and ADJUST was achieved only in one out of 14 subjects in study02. In nine of 14 subjects, the visual inspection selected two or three components. However, in ADJUST, usually, one of them did not meet predefined criteria and was not labeled as eye blink-related. Consequently, the overlap decreased to 50% (visual inspection - two components, ADJUST - one component) or 67% (visual inspection - three components, ADJUST - two components). The same was true for study03 and study04 - subjects falling into the category "overlap between 50% and 99%" usually differed in only one component, labeled as eye blink-related by visual inspection and not by ADJUST or vice versa.

Nevertheless, the ratio of subjects with an overlap between visual inspection and ADJUST above 50%, was above 0.6. What is more important, the visual inspection and ADJUST selected different components in only five out of 44 subjects in all four studies. In two of these five cases, ADJUST was not able to select any eye blink component, and therefore, its overlap with visual inspection was 0%.

When considering the overlap between visual inspection and the criterion based on correlation, the overlap was under 50% only in one of 44 subjects (subject from study04). Similarly to the ADJUST

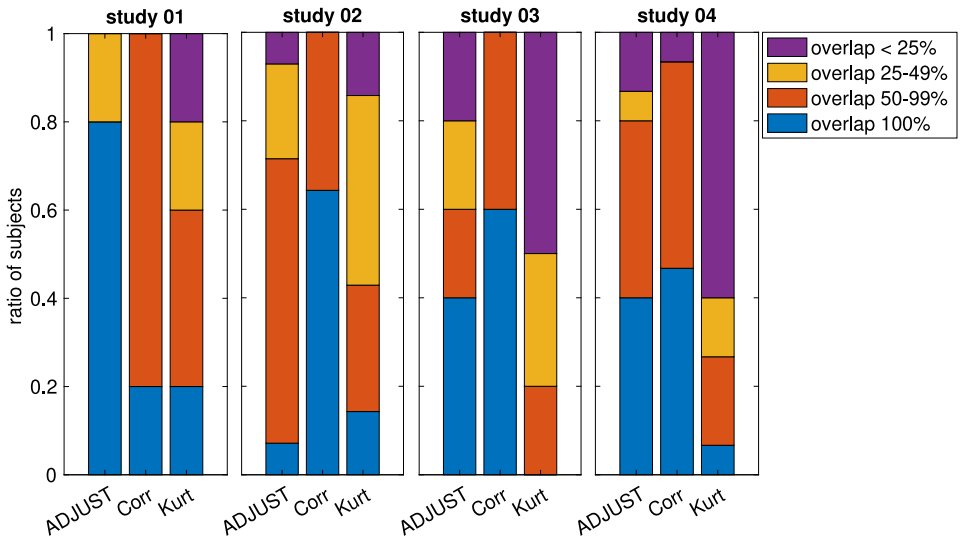

Fig. 11. The bar plot depicts the ratio of subjects (within each study) in which the overlap between visually selected eye blink components and the selection based on (i) ADJUST, (ii) correlation with EEG from frontal electrodes (Corr), and (iii) kurtosis of time scores (Kurt) was either 100% (exact overlap), between 50% and 99%, between 25% and 49%, or under 25%.

Table 2
For subjects in study 01, the eye blink related components were selected by (i) visual inspection of component time scores, spatial and frequency signatures, (ii) ADJUST algorithm, (iii) criterion based on correlation between component time scores and EEG signal from frontal electrodes above 0.4, and (iv) criterion based on time scores kurtosis above a given threshold. The "–" sign indicates, that any component was selected by the considered criterion.

Study 01	Number of gen.	Labels of selected components			
Subject	components	Visual insp.	ADJUST	Correlation	Kurtosis
1	3	1, 2	1, 2	1	–
2	4	1	1	1, 2	1
3	9	1, 2	1, 7	1, 2, 8	1, 7
4	6	1, 4	1, 4	1, 4	4
5	8	1, 2, 5, 7	1, 2, 5, 7	1, 5	5, 7

algorithm, selection based on visual inspection and correlation usually differed in only one or two of the selected components.

The most inconsistent results with visual selection were obtained for the criterion based on kurtosis. There are only four subjects with an exact match (Fig. 11), but also 17 subjects with overlap under 25%. Two reasons for these inconsistencies are: (i) the threshold proposed in [37] was too high in several cases and any kurtosis value overcame it (subject 01 from study01 in Table 2), or (ii) high kurtosis values were observed not only in TS of clearly eye blink-related components but also in components with TS following a peaky distribution, not representing eye blinks but some other type of artefacts. From this point of view, using a single criterion based on kurtosis for component selection may lead to inferior results, and we recommend combining its results with at least one other criterion.

Finally, we can conclude that visual inspection led to consistent results with both the automatic component selection criterion based on correlation and the ADJUST algorithm, which are widely used also for ICA eye blink component selection.

4.2. Comparison of ICA and SPECTER by using Dataset 2

4.2.1. Resting state epochs

As described in Section 3.3, we aimed to compute the Spearman's correlation coefficient between the original EEG signal and its versions corrected by SPECTER and ICA on resting state epochs. The median correlations for each subject and each electrode are depicted in Fig. 12. For the SPECTER algorithm we considered the eye blink-free EEG signal without correction for the slight time shift and opposite sign problem (Fig. 12, black dotted line) and its version after applying a heuristics described in Section 2.1 and the DTW algorithm (Fig. 12, black line).

Lower correlations between the EEG signal reconstructed by SPECTER and the original EEG during the resting state epochs were expected due to the slight time shift and opposite sign problem (Fig. 12, dotted line). After applying DTW and sign correction heuristics, the Spearman's correlations increased, and their median values were comparable with the correlations produced by ICA (Fig. 12, red line) for the majority of subjects and electrodes.

For subjects 6, 7, 8, and 9 in study02, ICA visually led to higher correlations for all electrodes than SPECTER with DTW. However, we would like to highlight that the achieved correlations between SPECTER with DTW and the original EEG signal were still high, at least 0.86, in these cases. Minor differences between SPECTER and ICA correlation values (at most 0.1) may be caused by the remaining opposite signs and slight time shift problems in SPECTER's EEG signal. As highlighted in Section 2.1, the proposed heuristics and DTW are promising but do not provide a 100% solution to both problems.

On the other hand, there are several subjects (Fig. 12, subjects 5, 8 in study04) for which ICA led to inferior frontal electrode results compared to SPECTER. In contrast to the situations described in the previous paragraph, in which SPECTER produced correlations above 0.86, in this case, ICA resulted in much lower correlations with the original EEG signal. We hypothesize that low correlations were caused by not negligible changes introduced by ICA during resting state epochs. An example for subjects 5 and 8 from study04 is depicted in Fig. 13. In this extreme case for subject 8, the correlation between the ICA corrected and original EEG signal was only 0.14 for electrode Fp1/AF3 and 0.16 for electrode F8.

The second measure considered was the absolute difference between the original EEG PSD and PSD of the signal corrected by SPECTER or ICA in four frequency bands. Using the nonparametric paired Wilcoxon test, we detected no significant difference between ICA and SPECTER in any frequency band (p-values were above $0.78 > 0.05$). This conclusion was true when merging the resting state epochs without eye blinks from one subject together and also when considering each epoch separately. From this point of view, SPECTER and ICA led to equivalent results.

Fig. 12. Dataset 2: The median Spearman's correlation coefficient between the original EEG signal and EEG signal reconstructed by SPECTER and ICA (red line) over rest epochs. In the case of SPECTER, the correlations were computed using only the SPECTER algorithm (black dotted line) or SPECTER followed by heuristics described in Section 2.1 and the DTW algorithm for solving the slight time shift and opposite sign problem (black line). Only labels for each second electrode are depicted on the x-axes.

4.2.2. Eye blink epochs

In the second step, we focused on eye blink epochs.[3] Since the true eye blink-free EEG signal is unknown over these epochs, we took the ICA results as a benchmark and computed Spearman's correlation coefficient between the eye blink-free EEG signal reconstructed by ICA and SPECTER over eye blink intervals. In the case of SPECTER, the reconstructed signal was also corrected for the opposite sign and slight time shift problem. The median correlations for each subject and each electrode are depicted in Figs. 14 and 15.

In most cases, SPECTER and ICA produced very similar results on parietal and occipital electrodes, mirrored in correlations above 0.8. Lower correlations, but still above 0.4, were observed on frontal electrodes. However, this was somewhat expected because frontal electrodes are affected mainly by eye blinks, and both ICA and SPECTER corrected them slightly differently. An example of one eye blink epoch for subject 5 from study04 is depicted in Fig. 16. Since the ground truth is unknown, we cannot decide which method removes the eye blinks "better".

Despite the lack of a clear winner in terms of eye blink removal, we can confidently conclude that SPECTER did not remove eye blinks in a significantly different way than ICA. This finding is significant, as it reinforces the main conclusion of our study. No negative or close to zero correlations were observed, further supporting this conclusion.

4.3. Comparison of Gratton-Coles & Donchin, ICA, and SPECTER by using Dataset 1

In the first step, we visually compared reconstructed signals using the GCD algorithm, ICA, and SPECTER. We can conclude that all three algorithms provided satisfactory results in most observations. In the following analysis, we would like to focus on selected results where differences between the methods were observed

An example of the EEG signal from the Fp1 electrode for Sub1_med2 is depicted in Fig. 17. The SPECTER algorithm removed eye blinks and provided visually satisfactory results similar to ICA (Fig. 17, left column). Both methods present a decrement in the spectrum of the reconstructed EEG signal compared to the original signal for low frequencies (Fig. 17, right column). However, the GCD algorithm faced difficulties because it could not wholly remove several eye blinks (Fig. 17, left column). The GCD reconstructed signal spectrum overestimates the spectrum of the original EEG signal for higher frequencies (Fig. 17, right column).

In the second step, we focused on a short time interval, including no visible eye blinks (Fig. 18). In this case, the original and reconstructed signals are assumed to overlap up to minor numerical differences. ICA provided the most similar reconstructed signal to the original one, and

[3] Only epochs originally labeled as eye blink were considered. The resting state epochs with eye blinks were not taken into account.

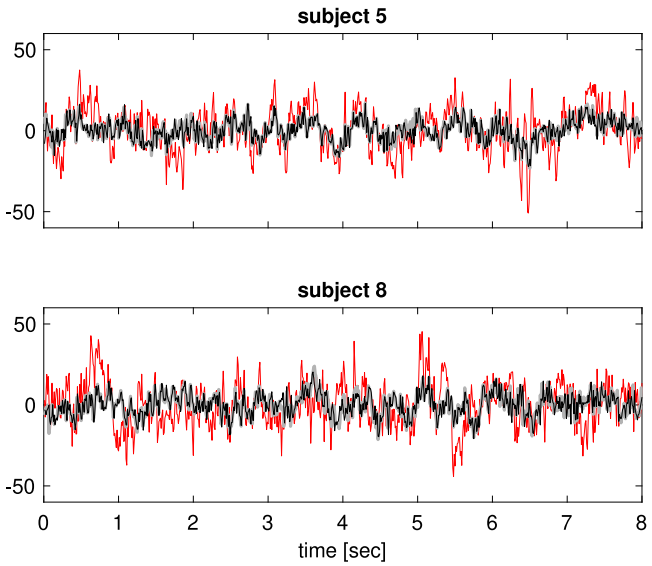

Fig. 13. Dataset 2: An example of the resting state EEG epoch from the Fp1 electrode of subjects 5 and 8 from study04 (gray) and its versions reconstructed by SPECTER with DTW (black) and ICA (red).

the corresponding spectra overlap. SPECTER also worked well. The difference between the original and GCD reconstructed signal spectrum was more extensive. We can conclude that GCD significantly changed the signal by adding an artificial component leading to spectrum overestimation. This result was confirmed by visual inspection of the GCD reconstructed signal (Fig. 18).

An opposite result was obtained for Sub3_post. In this case, SPECTER and GCD provided satisfactory results in both the time domain (Fig. 19, second and fourth row) and spectrum (Fig. 20). On the other hand, ICA was not able to remove the artifact at the very beginning of the observation and also in the second half of the time interval (Fig. 19, third row, left column). Moreover, the ICA-corrected EEG signal reaches higher amplitudes over both blink and non-blink time intervals leading to spectrum overestimation (Figs. 20 and 21, third row).

To quantify the observed differences by an objective measure, we computed the ratio between the spectrum of the reconstructed signal $\mathbb{X}_{reconstructed}$ and the original signal spectrum $\mathbb{X}_{orig}$. The original and reconstructed EEG signals were divided into 2-second time windows with 1.9 s of overlap (95%), and FFT computed the signal spectrum between 0 Hz and 30 Hz for each time window. Finally, the ratio was computed using the following formula

$$R^{el,f}_{spec} = \frac{\mathbb{X}^{el,f}_{reconstructed}}{\mathbb{X}^{el,f}_{orig}} \tag{4}$$

for each electrode el and each frequency f separately. If $R^{el,f}_{spec} \gg 1$, the spectrum of the reconstructed signal lies above the original signal spectrum - we speak about spectrum overestimation for a given electrode and a given frequency f.

The results for frontal EEG electrodes Fp1, Fp2, and Fz and nine EEG recordings where the spectrum overestimation occurred ($R_{spec} > 1$) are depicted in Fig. 22. We can see that both ICA and GCD overestimated the original signal spectrum in higher frequencies. Further analysis showed that the problem with spectra overestimation is present in data with a higher alpha rhythm amplitude (≈10 Hz–13 Hz). Still, more experiments and analysis are needed to confirm this observation. On the other hand, the ratio of the spectrum of the signal reconstructed by the SPECTER algorithm and the original signal spectrum is always under the threshold one.

4.3.1. A special situation when SPECTER is not appropriate

Both ICA and SPECTER algorithms are based on data variability analysis. Consequently, they can detect eye blink components only if there are satisfactory blink-free time intervals. However, this is not the case with the Sub1_post measurement, where the total duration of eye blinks overcomes the duration of non-blink intervals. As depicted in Fig. 23, ICA could not remove eye blinks. SPECTER produced better results than ICA, but the eye blinks are not entirely removed in the reconstructed signal. We hypothesize that due to the eye blink presence in most observations, both methods considered blinks (or a part of them) as a baseline. Consequently, they were not able to entirely remove them. For Sub1_post, only the GCD algorithm yielded satisfactory results because it is based on regression analysis instead of data variability (Fig. 23, top).

To confirm our hypothesis, we merged the original Sub1_post data with the signal reconstructed by the GCD algorithm and applied the SPECTER algorithm again. In this case, the new data included "enough" blink-free time intervals, and SPECTER successfully removed eye blinks present in the first half of the observation while remaining the second half unchanged (Fig. 24).

5. Conclusions

The present study deals with the problem of removing eye blinks from EEG signals. Traditional approaches like GCD [2] or ICA [8] perform well in a wide range of situations and under a variety of conditions. It is important to note, however, that both methods also possess certain disadvantages - an overestimation of the spectrum of the cleaned signal in ICA or removing valuable information from EOG by the GCD when EEG corrupts the EOG signal [4]. Therefore, when these traditional methods fail, finding an alternative approach to eye blink removal is practical.

In this study, we proposed the SPECTER algorithm combining tensor decomposition, namely the PARAFAC model, with the signal reconstruction from the amplitude spectrum [25]. The latent components obtained by the PARAFAC algorithm follow a natural physiological interpretation and are easily inspected for eye blink properties, either visually or mathematically. The component selection based on visual inspection provided similar results as two fully automated selection criteria proposed for ICA: (i) the ADJUST algorithm and (ii) the criterion based on the correlation between component time scores and the EEG signal from frontal electrodes.

Furthermore, the possible application of different constraints to the PARAFAC solution and the general nature of the overall algorithm allows the removal of a wide range of EEG artifacts or oscillatory rhythms, indicating that SPECTER is not limited only to eye blink EEG correction.

SPECTER was observed to provide a comparable ability to remove eye blinks with ICA and GCD algorithms when applied to EEG data from two datasets. But what is more critical, SPECTER provided superior performance in specific real-data situations, where ICA led to signal spectrum overestimation or GCD could not properly remove eye blinks.

A quantitative analysis based on correlations between the original EEG signal and EEG signal reconstructed by SPECTER across resting state and eye blink epochs from Dataset 2 led us to the conclusion that SPECTER did not change the EEG signal over resting-state epochs and produced comparable results with ICA. When comparing GCD's and SPECTER's performance on Dataset 1, we preferred a visual inspection over a quantitative analysis due to an unknown true eye blink-free EEG signal. Moreover, any quantitative comparison would be unfair since the EOG channel is essential in the GCD algorithm, but SPECTER does not need any EOG information. Moreover, SPECTER is also applicable when the EOG channel is unavailable.

The core idea of SPECTER is similar to the CWT-Tuc-OC algorithm [24], which is based on a combination of the wavelet transform with the Tucker model. However, the latent components extracted

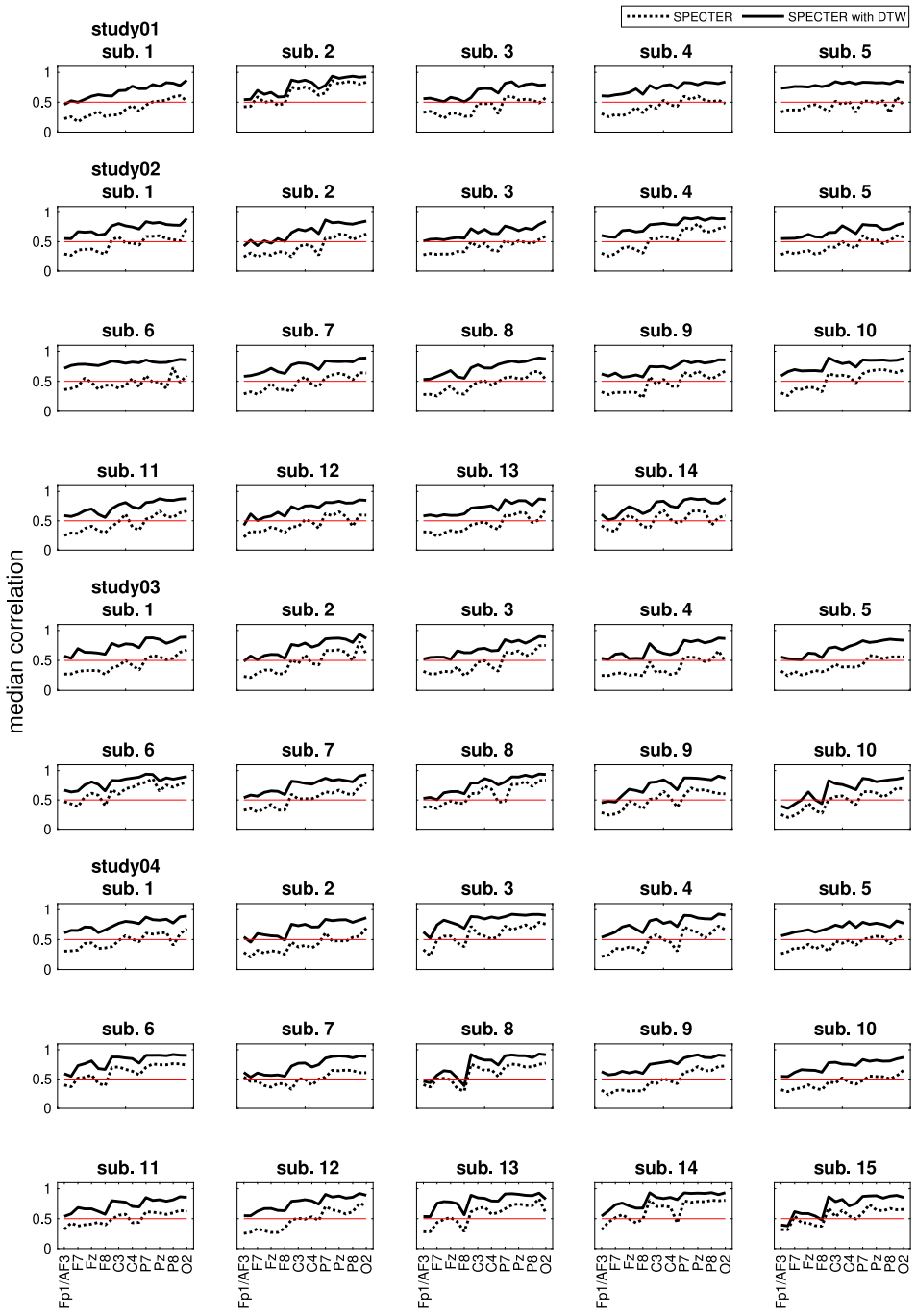

Fig. 14. Dataset 2: The median Spearman's correlation coefficient between EEG signal reconstructed by SPECTER and ICA over eye blink epochs. In the case of SPECTER, the correlations were computed by using only SPECTER algorithm (black dotted line) or SPECTER followed by heuristics described in Section 2.1 and DTW algorithm for solving the slight time shift and opposite sign problem (black line). Only labels for each second electrode are depicted on the x-axes.

from the wavelet coefficient tensor do not follow a natural interpretation in the spatial and pseudo-frequency domain. Only the time scores can be used for the eye blink-related components selection. Despite our effort to properly tune CWT-Tuc-OC parameters and different approaches to select and remove eye blink-related components, CWT-Tuc-OC produced inferior results to SPECTER.

Nevertheless, SPECTER was also observed to have some shortcomings, allowing space for future improvement. Since the tensor decomposition is based on data variability analysis, SPECTER is inappropriate for EEG signals with insufficient eye blink-free time intervals.

The second disadvantage of SPECTER is the presence of slight time shifts and opposite signs in the reconstructed signal values due to the need for more information about the signal phase spectrum. In this study, we proposed simple heuristics to solve the opposite sign problem. The slight time shifts may diminish after applying a time-warping method. Nevertheless, these two problems are present only when analyzing the resulting eye blink-free signal in the time domain. In practice, the EEG analysis usually focuses on the signal spectrum and properties in the time-frequency or time-space-frequency domain rather than the raw signal. Consequently, it is possible to omit the fourth step in SPECTER's algorithm since X_{rem} from Section 2 already represents the spectrum of eye blink-free signal.

To conclude, this study aims not to compete with ICA, GCD, or other eye blink removal approaches, whose good performance has been

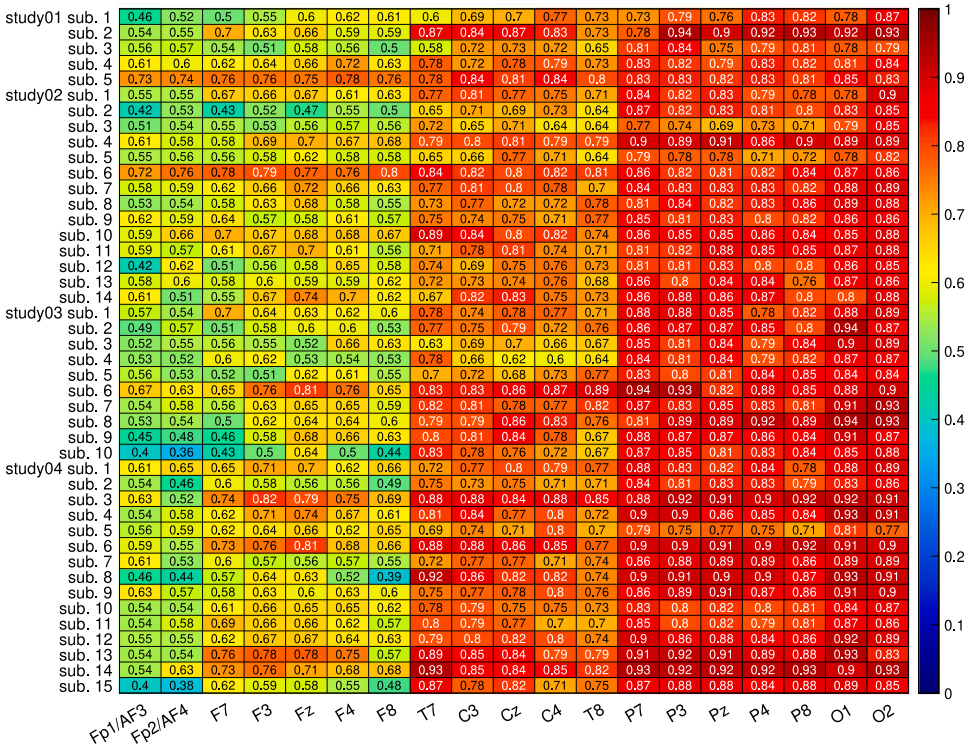

Fig. 15. Dataset 2: Heatmaps depicting the median Spearman's correlation coefficient between EEG signal reconstructed by ICA and SPECTER followed by heuristics described in Section 2.1 and DTW algorithm for solving the slight time shift and opposite sign problem over eye blink epochs.

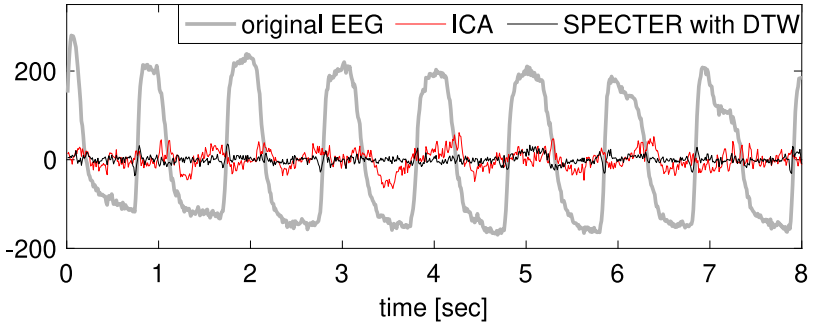

Fig. 16. Dataset 2: An example of the eye blink EEG epoch from the Fp1 electrode of subject 5 from study04 (gray) and its versions reconstructed by SPECTER with DTW (black) and ICA (red).

proven in the literature. We propose the SPECTER algorithm as an alternative method where traditional algorithms may fail or identification of the latent eye blink tensor components is preferred while inspecting EEG data. Despite the pilot nature of the presented results and room for further algorithm improvement, SPECTER offers a promising way to solve the eye blink removal problem.

CRediT authorship contribution statement

Zuzana Rošťáková: Writing – review & editing, Writing – original draft, Visualization, Validation, Software, Methodology, Formal analysis, Data curation, Conceptualization. **Roman Rosipal:** Writing – review & editing, Writing – original draft, Supervision, Methodology, Conceptualization. **Leonardo Jose Trejo:** Writing – review & editing, Writing – original draft, Supervision, Methodology.

Declaration of competing interest

The authors declare that they have no known competing financial interests or personal relationships that could have appeared to influence the work reported in this paper.

Data availability

Data will be made available on request.

Acknowledgments

This research was supported by the Recovery and Resilience Plan Funding: Fellowships for excellent researchers R2-R4 (grant 09I03-03-V04-00205), Scientific Grant Agency of the Ministry of Education, Research, Development and Youth of the Slovak Republic and Slovak Academy of Sciences VEGA (grant 2/0023/22), by the Slovak Research and Development Agency (grant APVV-21-0105) and by the CHIST-ERA 20-BCI-004 grant. We would like to thank Bartłomiej Stasiak for his suggestion to solve the problem of slight time shifts present in the reconstructed EEG signal.

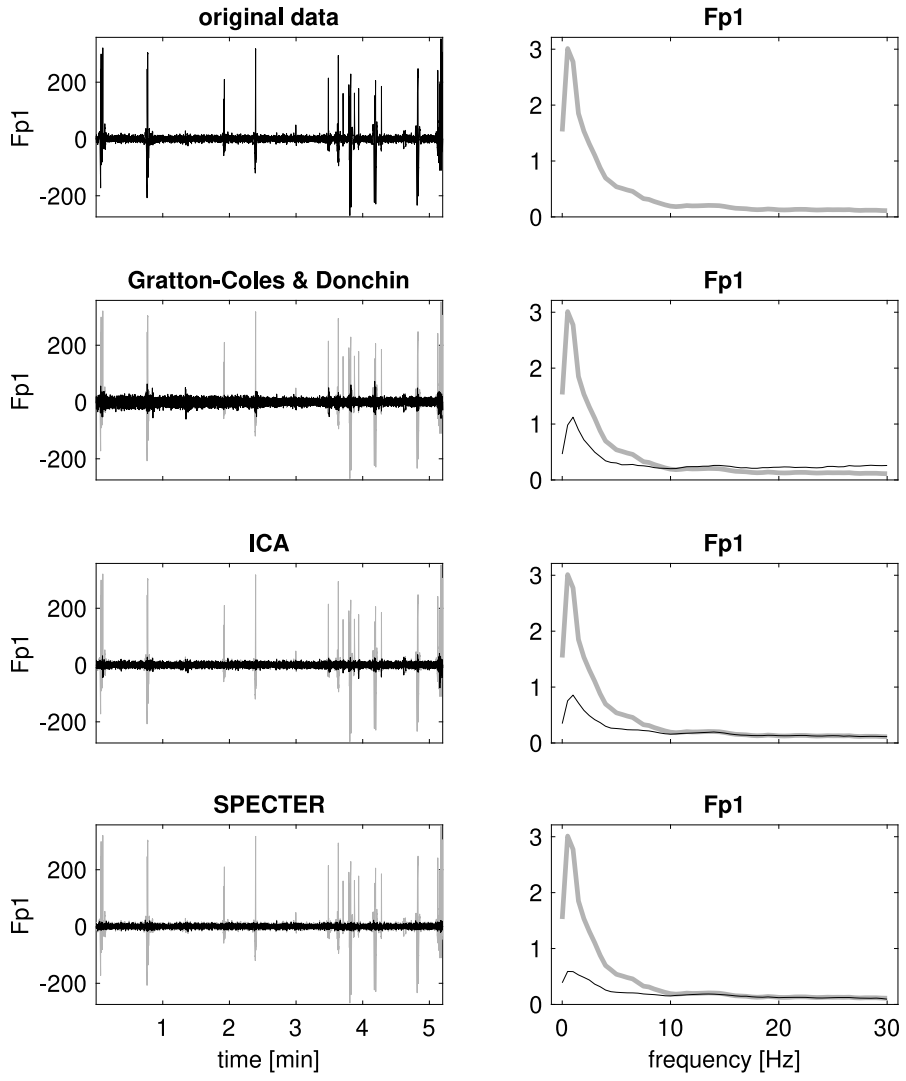

Fig. 17. Sub1_med2: The original Fp1 electrode EEG signal and EEG signals reconstructed by the Gratton-Coles & Donchin, ICA, and SPECTER algorithms (left column). The right column depicts the corresponding normalized amplitude spectrum. For a better comparison, subfigures with reconstructed signal (black) also include the original EEG signal or its spectrum (gray).

Appendix A. Removing components in PARAFAC and Tucker model

Let us assume the estimated component matrices $A^{(1)}, \dots, A^{(N)}$, and the super-diagonal core tensor $\underline{G}$ either in PARAFAC (2) or in the Tucker model (1). In the following text, three approaches for the eye blink removal from the data tensor $\underline{X}$ are described.

(i) signature zeroing. In the first approach, the component signatures following eye blink characteristics are set to a zero vector of appropriate length. Let us denote the modified component matrices as

$$A^{(n)\star} = \left(\mathbf{a}_1^{(n)\star} \mathbf{a}_2^{(n)\star} \dots \mathbf{a}_F^{(n)\star}\right);$$

$$\mathbf{a}_f^{(n)\star} = \begin{cases} \mathbf{a}_f^{(n)}, & f \notin S_{rem}^{(n)}, \\ \mathbf{0}, & f \in S_{rem}^{(n)}, \end{cases} \qquad f = 1, \dots, F,$$

where $S_{rem}^{(n)}$ is an index set of signatures selected for zeroing in the nth mode.

The formula for the "cleaned" tensor $\underline{X}_{rem}$ by using the Tucker model follows

$$\underline{X}_{rem} = \sum_{k_1=1}^{K_1} \sum_{k_2=1}^{K_2} \cdots \sum_{k_N=1}^{K_N} g_{k_1 k_2 \dots k_N} \mathbf{a}_{k_1}^{(1)\star} \circ \mathbf{a}_{k_2}^{(2)\star} \circ \dots \circ \mathbf{a}_{k_N}^{(N)\star}$$

$$= \sum_{k_1 \notin S_{rem}^{(1)}} \sum_{k_2 \notin S_{rem}^{(2)}} \cdots \sum_{k_N \notin S_{rem}^{(N)}} g_{k_1 k_2 \dots k_N} \mathbf{a}_{k_1}^{(1)} \circ \mathbf{a}_{k_2}^{(2)} \circ \dots \circ \mathbf{a}_{k_N}^{(N)}. \tag{A.1}$$

Due to the diagonal structure of the core tensor $\underline{G}$ in the PARAFAC model (2), zeroing an fth signature in the nth mode leads to its zeroing in other modes as well. Let us denote $S_{rem} = \cup_{n=1}^{N} S_{rem}^{(n)}$. Consequently, Eq. (A.1) simplifies to

$$\underline{X}_{rem} = \sum_{f=1}^{F} g_{f \dots f} \mathbf{a}_f^{(1)\star} \circ \dots \circ \mathbf{a}_f^{(N)\star} = \sum_{f \notin S_{rem}} g_{f \dots f} \mathbf{a}_f^{(1)} \circ \dots \circ \mathbf{a}_f^{(N)}. \tag{A.2}$$

In other words, $\underline{X}_{rem}$ is reconstructed using only the non-artifactual components.

This approach for the Tucker model was used in the CWT-Tuc-OC algorithm [24]. However, signature zeroing does not consider the possible error of PARAFAC or the Tucker model itself, see Eqs. (2) and (1). If the model is inappropriate and the error still includes significant useful information and data variation, this information will also be missing in $\underline{X}_{rem}$. The problem will be demonstrated in detail in Appendix A.1.

(ii) component subtraction. Component subtraction for PARAFAC is described in Section 1.3, so let us consider the Tucker model.

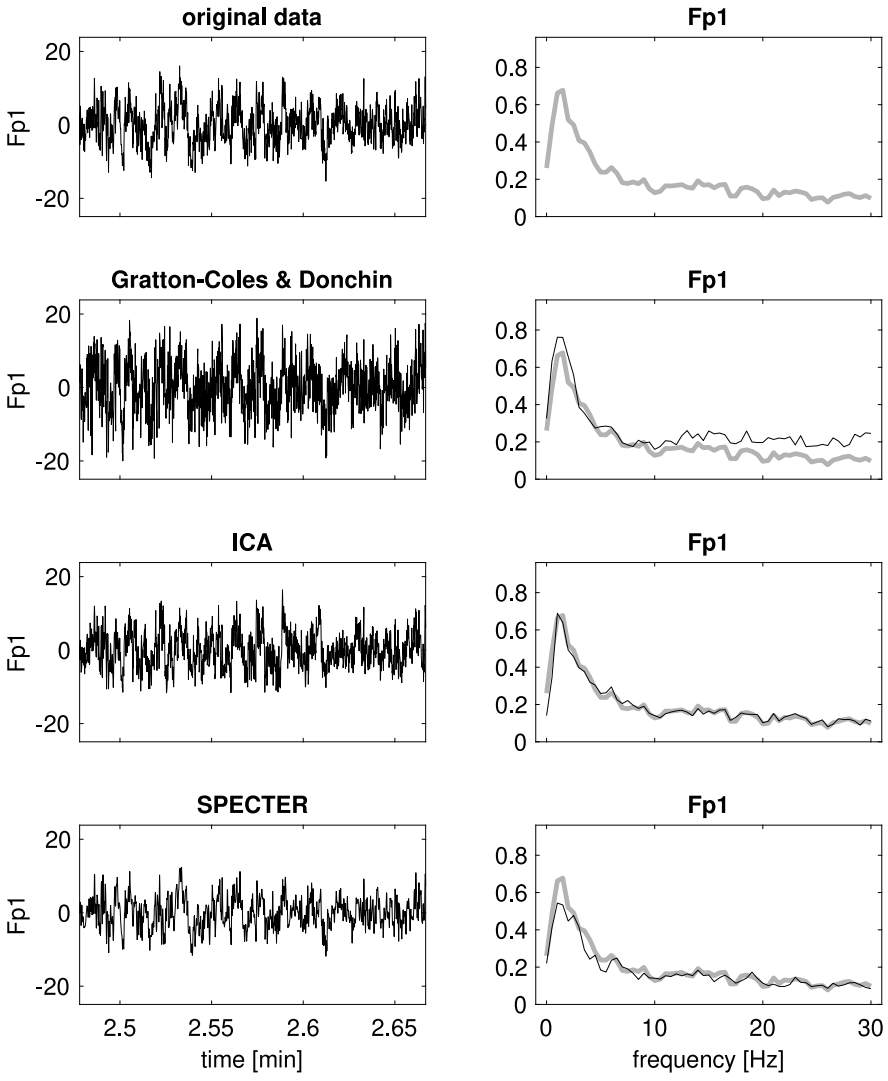

Fig. 18. Sub1_med2: A selected interval of the original Fp1 electrode EEG signal (top left) and EEG signals reconstructed by Gratton-Coles & Donchin, ICA, and SPECTER algorithms (left column). The right column depicts the corresponding normalized amplitude spectra of the original EEG signal (gray) and of the eye blink corrected signal (black). The interval was selected so the original EEG signal includes no eye blinks.

Subtraction in one, for example the mth mode, is straightforward

$$\underline{X}_{rem} = \underline{X} - \sum_{k_1=1}^{K_1} \cdots \sum_{k_m \in S_{rem}^{(m)}} \cdots \sum_{k_N=1}^{K_N} g_{k_1 \ldots k_m \ldots k_N} \mathbf{a}_{k_1}^{(1)} \circ \ldots \circ \mathbf{a}_{k_m}^{(m)} \circ \ldots \circ \mathbf{a}_{k_N}^{(N)}.$$

Subtraction in several modes is more complex. For simplicity, let us assume only the first and second modes. In the first case, only components with the first mode signature belonging to $S_{rem}^{(1)}$ and the second mode signature belonging to $S_{rem}^{(2)}$ are removed

$$\underline{X}_{rem_1} = \underline{X} - \sum_{k_1 \in S_{rem}^{(1)}} \sum_{k_2 \in S_{rem}^{(2)}} \sum_{k_3=1}^{K_3} \cdots \sum_{k_N=1}^{K_N} g_{k_1 k_2 k_3 \ldots k_N} \mathbf{a}_{k_1}^{(1)} \circ \mathbf{a}_{k_2}^{(2)} \circ \mathbf{a}_{k_3}^{(3)} \circ \ldots \circ \mathbf{a}_{k_N}^{(N)}.$$

On the other hand, it is also possible to remove all components with either the first mode signature from $S_{rem}^{(1)}$ or the second mode signature from $S_{rem}^{(2)}$

$$\underline{X}_{rem_2} = \underline{X} - \sum_{k_1 \notin S_{rem}^{(1)}} \sum_{k_2 \in S_{rem}^{(2)}} \sum_{k_3=1}^{K_3} \cdots \sum_{k_N=1}^{K_N} g_{k_1 k_2 k_3 \ldots k_N} \mathbf{a}_{k_1}^{(1)} \circ \mathbf{a}_{k_2}^{(2)} \circ \mathbf{a}_{k_3}^{(3)} \circ \ldots \circ \mathbf{a}_{k_N}^{(N)} -$$
$$- \sum_{k_1 \in S_{rem}^{(1)}} \sum_{k_2 \notin S_{rem}^{(2)}} \sum_{k_3=1}^{K_3} \cdots \sum_{k_N=1}^{K_N} g_{k_1 k_2 k_3 \ldots k_N} \mathbf{a}_{k_1}^{(1)} \circ \mathbf{a}_{k_2}^{(2)} \circ \mathbf{a}_{k_3}^{(3)} \circ \ldots \circ \mathbf{a}_{k_N}^{(N)} -$$
$$- \sum_{k_1 \in S_{rem}^{(1)}} \sum_{k_2 \in S_{rem}^{(2)}} \sum_{k_3=1}^{K_3} \cdots \sum_{k_N=1}^{K_N} g_{k_1 k_2 k_3 \ldots k_N} \mathbf{a}_{k_1}^{(1)} \circ \mathbf{a}_{k_2}^{(2)} \circ \mathbf{a}_{k_3}^{(3)} \circ \ldots \circ \mathbf{a}_{k_N}^{(N)}.$$

The choice of $\underline{X}_{rem_1}$ or $\underline{X}_{rem_2}$ depends on the user preferences and overall interpretability. Considering more than two modes leads to similar, only more complicated formulas.

(iii) projection to nullspace to the space spanned by selected signatures. The third approach for signature removal differs from the previous two and was inspired by [22].

The PARAFAC model solution is unique up to a component order [32]. The same is true for the Tucker model. Therefore, let us permute the component matrix columns and corresponding fibers in $\underline{G}$ so as the first $M_n < K_n$ signatures in the nth, $n = 1, \ldots, N$ mode are those we would like to remove and let us divide the component matrices into two blocks

$$A^{(n)} = \left(B^{(n)}, \quad C^{(n)}\right), \qquad n = 1, \ldots, N,$$

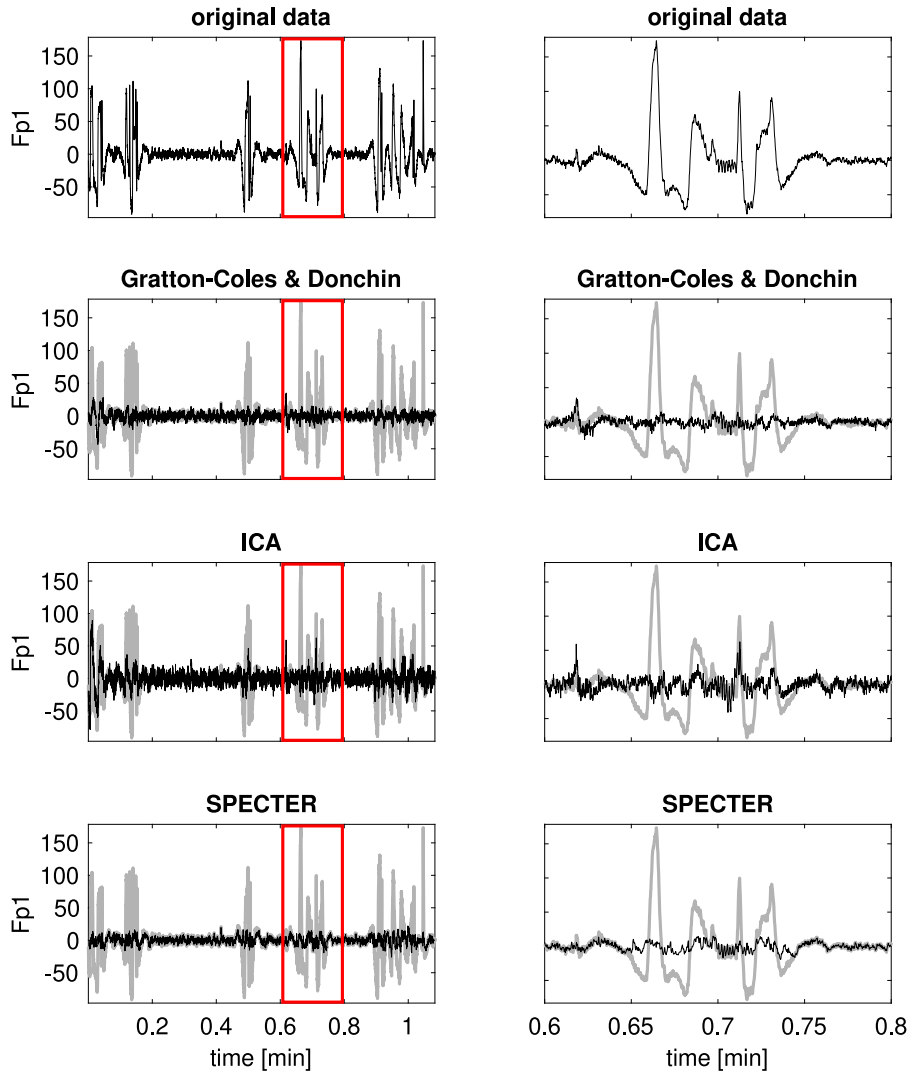

Fig. 19. Sub3_post: The original Fp1 electrode EEG signal and EEG signals reconstructed by the Gratton-Coles & Donchin, ICA, and SPECTER algorithms (left column). The right column shows a detailed view of a short time interval including eye blinks (red rectangle in the left column). For a better comparison, subfigures with reconstructed signal (black) also include the original EEG signal (gray).

$$B^{(n)} \in \mathbb{R}^{J_n \times M_n}, \qquad B^{(n)} = \left(\mathbf{a}_1^{(n)}, \mathbf{a}_2^{(n)}, \dots, \mathbf{a}_{M_n}^{(n)}\right),$$

Then

$$\underline{X}_{rem} = \underline{X} \times_{n_1} P_{n_1} \times_{n_2} P_{n_2} \dots \times_{n_V} P_{n_V},$$

where $n_1, n_2, \dots, n_V$ are modes in which the signature projection is performed, $P_{n_v} = \mathbb{I}_{J_{n_v}} - B^{(n_v)} B^{(n_v)^+}$ is a projection matrix to the nullspace of space spanned by the $B^{(n_v)}$ columns, and $B^{(n_v)^+}$ represents the Moore–Penrose pseudo-inverse of $B^{(n_v)}$. The order of tensor-matrix products in different modes is arbitrary [26].

In contrast to the previous two approaches, deciding in which mode or modes the projection is performed is important. Let us consider the projection in the first mode and the PARAFAC model

$$\underline{X}_{rem} = \underline{X} \times_1 P_1 = \underline{X} \times_1 \left(\mathbb{I}_{J_1} - B^{(1)} B^{(1)^+}\right).$$

By using the mode-1 unfolding, this can be rewritten in the following form

$$\begin{aligned} \underline{X}^{rem}_{(1)} &= P_1 X_{(1)} \\ &= P_1 A^{(1)} G_{(1)} \left(A^{(n)} \odot A^{(n-1)} \odot \dots \odot A^{(2)}\right)^T + P_1 E_{(1)} \\ &= \left(\mathbb{O}_{J_1 \times M}, \quad P_1 C^{(1)}\right) G_{(1)} \left(A^{(n)} \odot A^{(n-1)} \odot \dots \odot A^{(2)}\right)^T + P_1 E_{(1)}. \end{aligned}$$

After transforming back into the tensor form, we obtain

$$\begin{aligned} \underline{X}_{rem} &= \sum_{f=1}^{M} g_{ff\dots f} \mathbf{0} \circ a_f^{(2)} \circ \dots \circ a_f^{(n)} + \\ &+ \sum_{f=M+1}^{F} g_{ff\dots f} \left(P_1 a_f^{(1)}\right) \circ a_f^{(2)} \circ \dots \circ a_f^{(n)} + \underline{E} \times_1 P_1 = \\ &= \sum_{f=M+1}^{F} g_{ff\dots f} \left(P_1 a_f^{(1)}\right) \circ a_f^{(2)} \circ \dots \circ a_f^{(n)} + \underline{E} \times_1 P_1. \end{aligned}$$

We can see that the first M components are successfully removed as requested. However, the remaining first mode signatures are transformed by the P_1 multiple. Signatures in other modes $(2, 3, \dots, N)$ remain unchanged.

This result can be easily generalized to the Tucker model and to situations when the projection is performed in the $n_1^{th}, n_2^{th}, \dots, n_V^{th}$ modes.

A.1. Comparison of the component removal methods in SPECTER

This section discusses the performance of three component removal approaches described in Section 1.3 and Appendix A. Because we decided to use the PARAFAC model in SPECTER, we focus only on

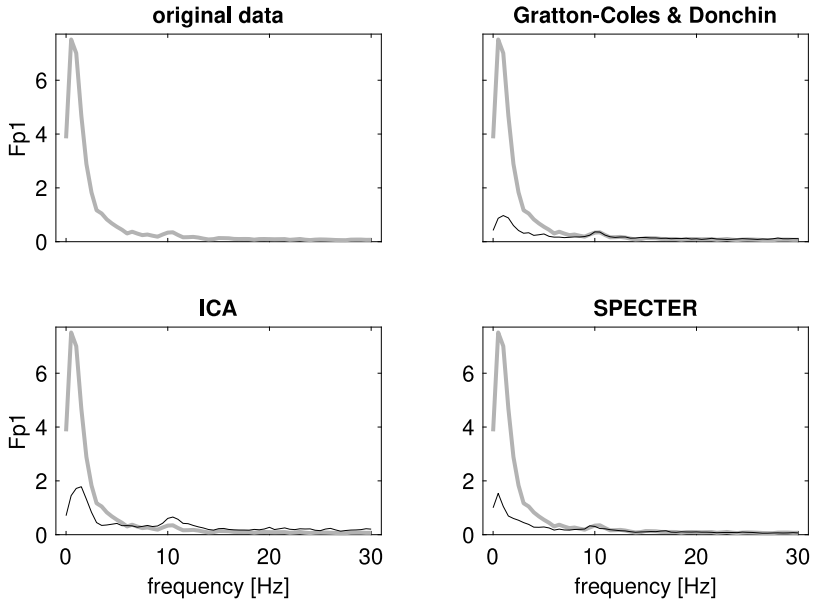

Fig. 20. Sub3_post: Normalized amplitude spectra of the original EEG signal (gray) and of the eye blink corrected signal (black) for the short time interval including eye blinks from Fig. 19.

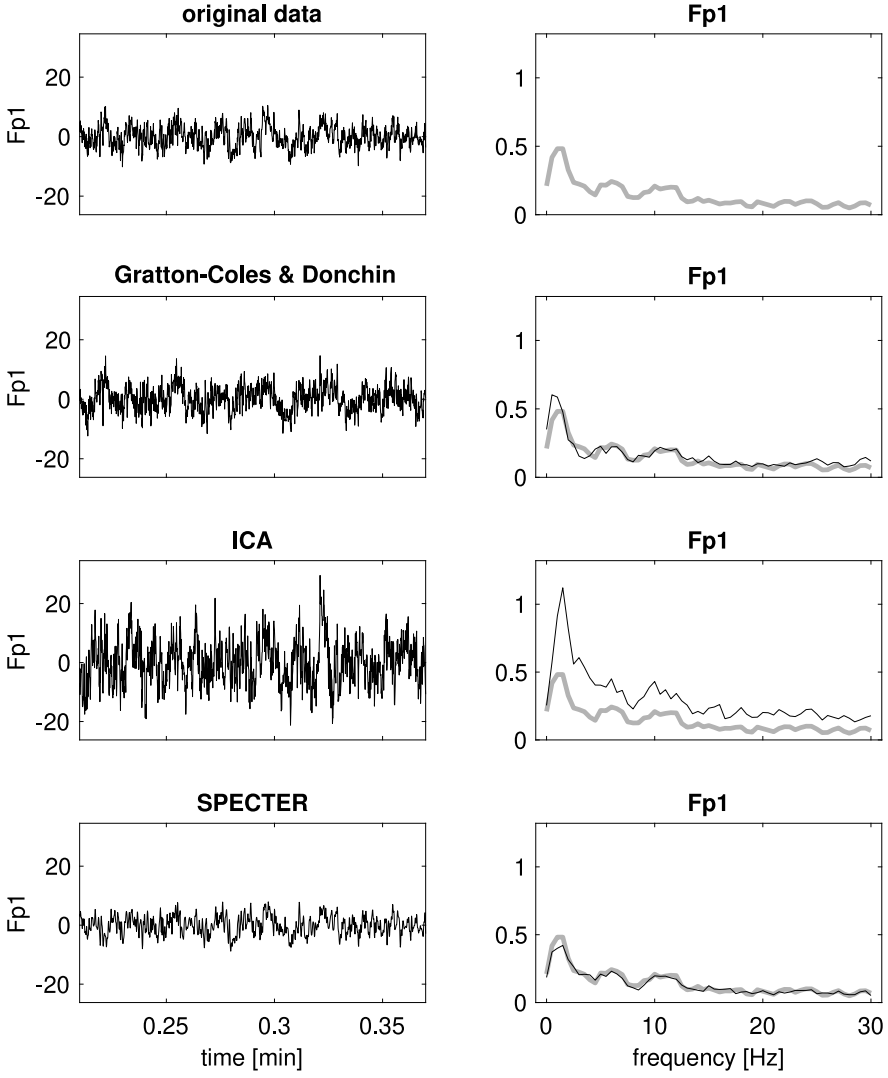

Fig. 21. Sub3_post: See Fig. 18 description.

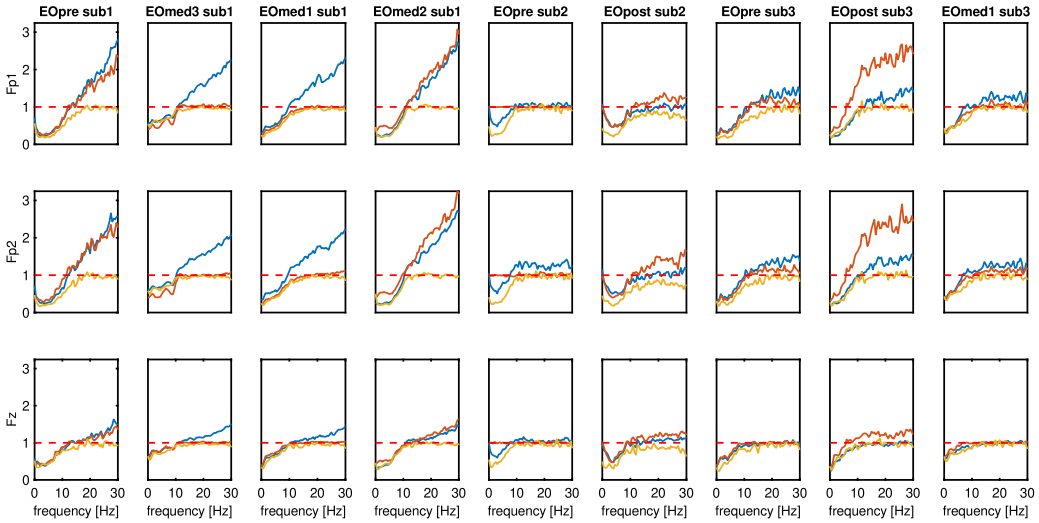

Fig. 22. The ratio of the eye blink-free EEG spectrum and original EEG spectrum at the frontal Fp1, Fp2, and Fz EEG electrodes. Eye blinks were removed by using the Gratton-Coles & Donchin (blue), ICA (orange), and SPECTER (yellow) algorithms.

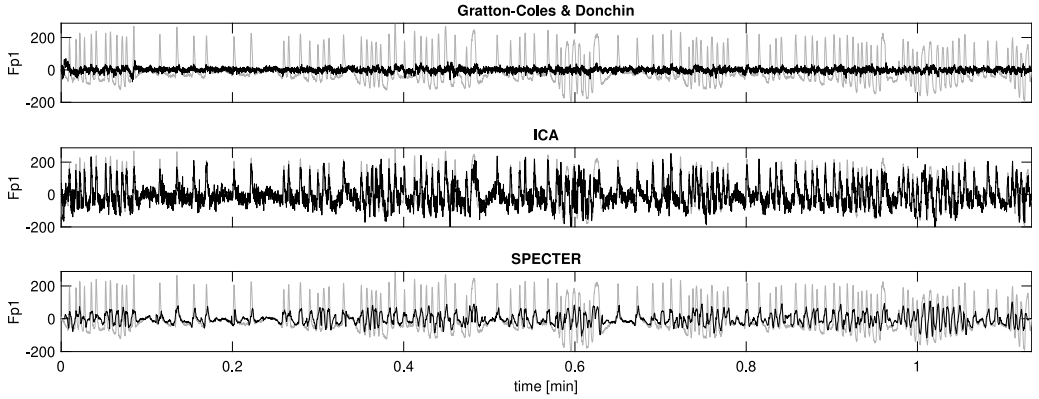

Fig. 23. Sub1_post: Original EEG signal (gray) and EEG signal reconstructed by the Gratton-Coles & Donchin, ICA, and SPECTER algorithms (black) at the Fp1 electrode of Subject 1 from the post-meditation EEG recording.

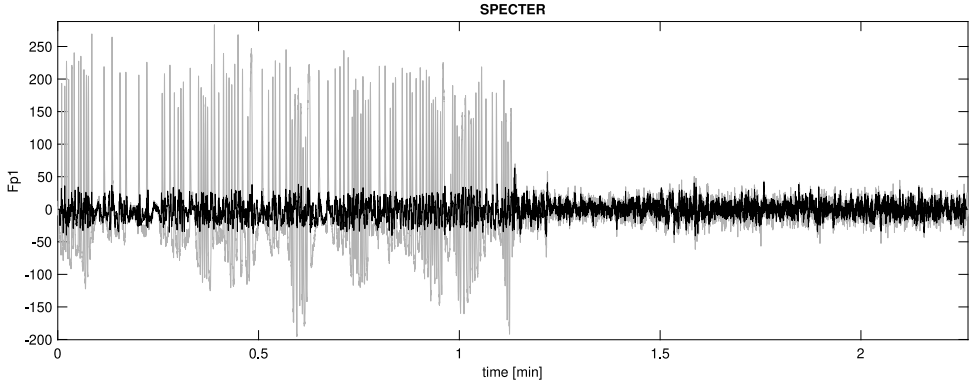

Fig. 24. Sub1_post: EEG data constructed by merging the original EEG signal of Subject 1 after meditation (Sub1_post) with its reconstruction by the Gratton-Coles & Donchin algorithm from Fig. 23 (gray). In this case, the data includes enough blink-free time intervals, and the SPECTER algorithm can remove eye blinks present in the first half of the data (black).

the component removal versions for PARAFAC. The results are demonstrated by using the Sub1_med3 data, but similar phenomena were also observed for all other data from Section 3.

General atoms for Sub1_med3 obtained by the *tripleC* cluster analysis are depicted in Fig. A.25. The first two components were selected as eye blink related because they represent brain activity in the frontal region and at low frequencies. Moreover, higher values of their time scores visually correspond with the eye blink position in the EEG signal from the Fp1 electrode. This is also supported by the observed statistically significant correlations between time scores and absolute amplitudes of the Fp1 signal.

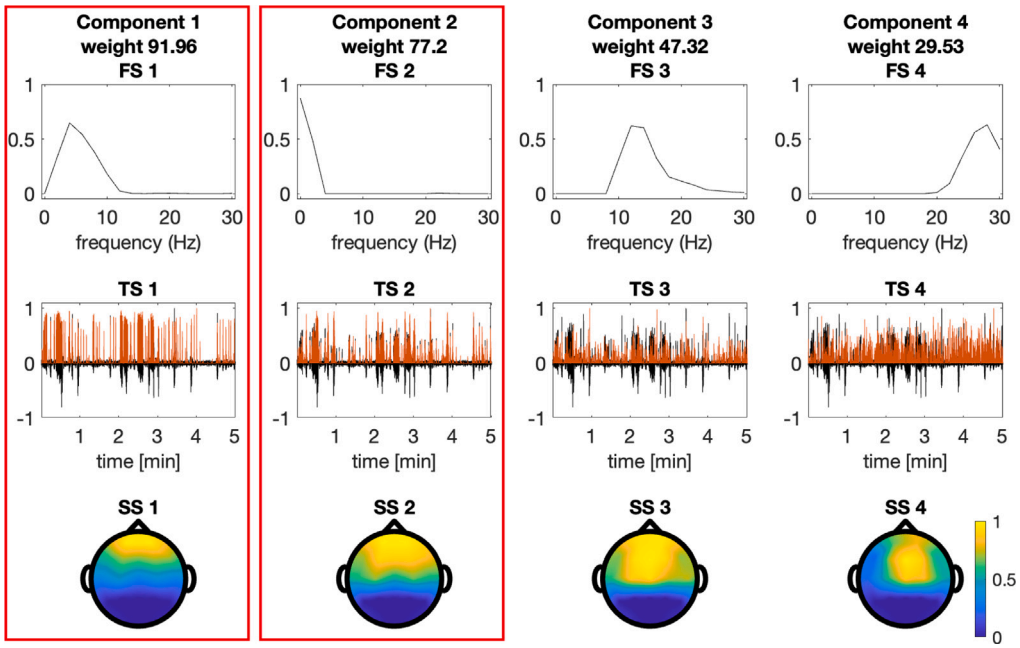

Fig. A.25. Sub1_med3: General components (columns) detected by the cluster analysis of PARAFAC model with one to ten components - the *tripleC* algorithm. The frequency signatures (FS) are depicted in the first row together with the component weight (the corresponding diagonal elements of the core tensor $\underline{G}_c$ (3)) in the title. The time scores (TS, orange) are compared with the original EEG signal from the Fp1 electrode (black) in the second row. Spatial signatures (SS) are plotted as topographic maps with the same color scale in the third row. Two components representing eye blinks and selected for removal within the SPECTER algorithm are highlighted by red rectangles.

Following the component removal description in Section 1.3, we considered five cases: (i) component zeroing, (ii) component subtraction, (iii) projection in the first (temporal) mode, (iv) projection in the second (spatial) mode, and (v) projection in the third (frequency) mode. A combined projection within two or all three modes did not bring any significant improvement; therefore, the results are not presented in this study.

In the component zeroing approach, the reconstructed signal is created only by the non-artifactual general components. For Sub1_med3, it is the third and the fourth component depicted in Fig. A.25. However, this approach does not consider the information in the PARAFAC model error. Consequently, the reconstructed signal looks like a straight line with close-to-zero values (Fig. A.26, top). These two signals' different behavior was observed on shorter intervals without eye blinks. Differences became even more visible after signal normalization to unit maximum (Fig. A.27, top). The same results were also observed for other real EEG data. Therefore, component zeroing is inappropriate for the SPECTER algorithm.

Regarding the component projection approach, spatial or frequency mode projection led to visually similar results like in component zeroing (Fig. A.26). The original and reconstructed signals should overlap over non-blink time intervals, but this is not the case, neither after normalization to unit maximum (Fig. A.27). We can conclude that spatial or frequency mode projection is also unsuitable for SPECTER.

The best results were obtained with projection in the first mode or component subtraction (Fig. A.26). In both cases, the reconstructed signal overlap with the original signal over the non-blink intervals, except for some sign changes (Fig. A.27). However, we observed a problem with the projection in the first mode when focusing on a short time interval, including several eye blinks. As depicted in Fig. A.28 (bottom), the original and reconstructed signal overlap on short intervals between blinks. But during a blink, the reconstructed signal is close to a straight line by removing too much information from the original signal.

On the other hand, this problem is not present in the component subtraction approach (Fig. A.28, top). Despite the missing eye blink free version of data, we can conclude that the signal reconstructed by SPECTER with component subtraction follows visually more realistic EEG signal properties compared to a situation when the first mode projection is used. Therefore, this study uses only component subtraction in the SPECTER algorithm.

Appendix B. Eye blink removal by the CWT and Tucker model

In this section, we focus on the CWT-Tuc-OC algorithm [24] due to its similarity to SPECTER.

The continuous wavelet transform (CWT) with the Morlet mother wavelet and various scales is applied to the min–max normalized EEG signal in the first step. Since no information about the data tensor construction is provided in [24], we assume that the wavelet coefficients are directly concatenated into the *time points* × *space (electrodes)* × *scales* tensor. This assumption is partially confirmed also by the application of inverse CWT in the last step of the algorithm, which would be difficult to perform if the coefficients are transformed, for example, the square absolute values of CWT coefficients used in [11,22].

In the second step, an unconstrained Tucker model from the Tensor-Toolbox [51] with the same number of signatures in each mode [24, Section 2.2] is applied. The estimated temporal mode signatures with the absolute value of either normalized entropy or kurtosis above a given threshold 1.5 are assumed to represent eye blinks [24].

Then, the selected signatures are replaced by zero vectors resulting in a modified time component matrix. The eye blink free tensor is constructed by tensor-matrix multiplication of the estimated core tensor, space, scales component matrices, and modified time component matrix. For more details, see the component zeroing in the Tucker model in Appendix A. Finally, the eye blink free signal is reconstructed by the inverse CWT. However, due to min–max normalization performed before CWT, the reconstructed signal must be multiplied by an appropriate multiple to have comparable amplitudes with the original EEG signal on non-blink time intervals.

Despite many similarities between [24] and SPECTER, we would like to highlight several differences:

1. **tensor construction and interpretability:** SPECTER focuses on the amplitude spectrum of the windowed EEG signal in the tensor construction step and allows for a natural interpretation

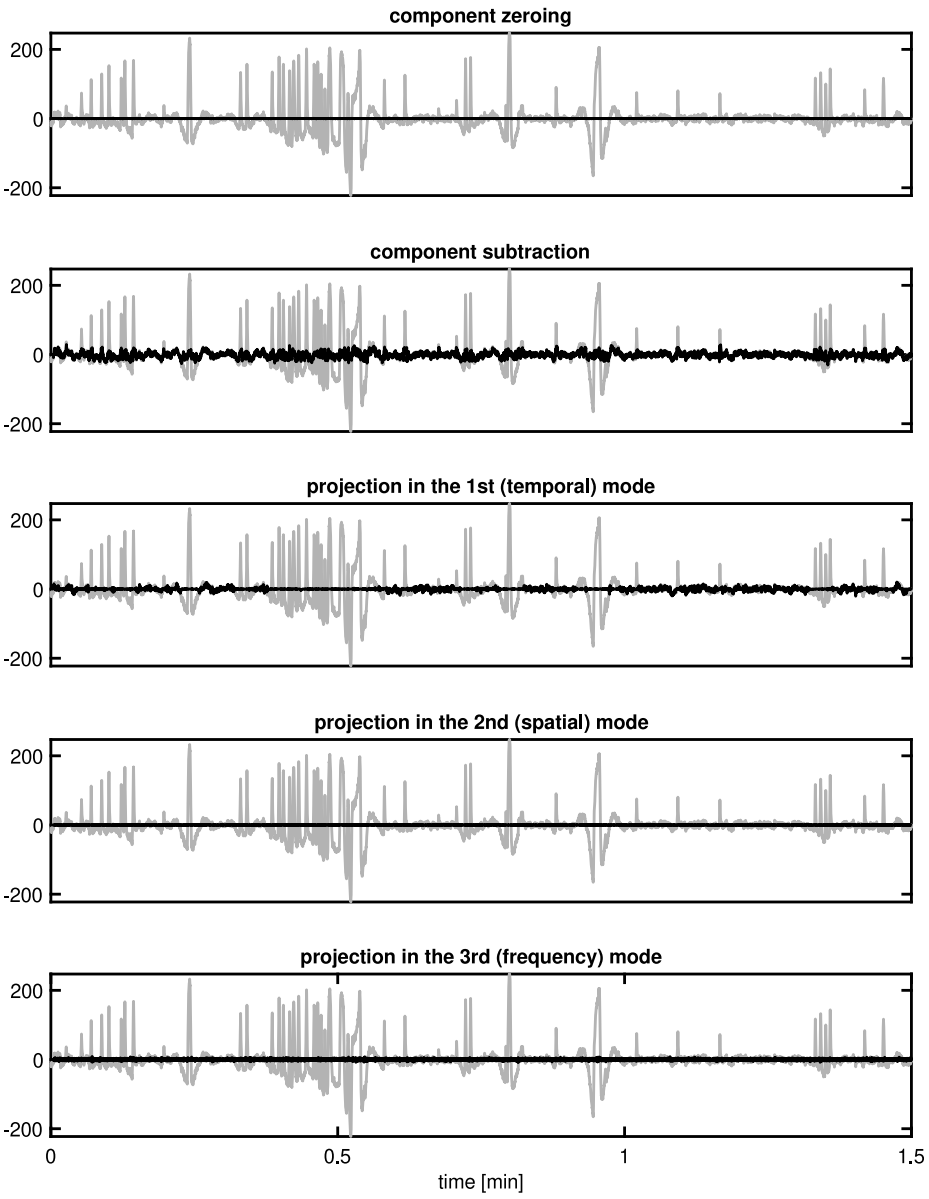

Fig. A.26. Sub1_med3: Comparison of the original, eye blink contaminated EEG signal (gray) from the Fp1 electrode and signal reconstructed by the SPECTER algorithm (black) with (i) component zeroing, (ii) component subtraction, (iii) projection in the first (temporal) mode, (iv) projection in the second (spatial) mode, and (v) projection in the third (frequency) mode. To better highlight the differences between original and reconstructed signals, only the first 1.5 min of the signal is shown.

in all three modes. CWT-Tuc-OC uses the continuous wavelet transform [24], and the scales or pseudofrequencies are usually more challenging to interpret.

2. **tensor size and computational complexity of tensor decomposition:** In CWT-Tuc-OC, the tensor has the size *number of time points* × *number of electrodes* × *number of scales*. Consequently, a high sampling frequency with a longer EEG measurement may significantly increase the power complexity of tensor decomposition and computational time, eventually leading to memory overflow.[4] Nevertheless, this problem can be partially solved by downsampling [11,22]. In SPECTER, the tensor size is *number of time windows* × *number of electrodes* × *number of frequencies*, where *number of time windows* ≪ *number of time points*.
3. **tensor nonnegativity:** The tensor constructed from the amplitude spectrum is naturally nonnegative, but no signature removal approach can preserve this property. Therefore, the log_{10} transformed tensor is used in tensor decomposition, and after signature removal, the inverse transformation (power of 10) is applied. On the other hand, this intermediate (transformation) step is not necessary in CWT-Tuc-OC.
4. **component inspection:** In SPECTER, we analyze the temporal, spatial, and frequency signatures simultaneously, and only components which follow artifact characteristics in all three signatures are considered in the artifact removal step. On the other hand, CWT-Tuc-OC focuses only on the temporal signatures [24].
5. **phase information:** Due to the lack of the phase spectrum information, the SPECTER's reconstructed signal may include values with opposite signs over short intervals. Nevertheless, this problem can be partially solved with simple heuristics described in Section 2.1. This problem is not present in CWT-Tuc-OC.

[4] For example, we were not able to run a Tucker model for a 5-minute long real EEG signal with a 128 Hz sampling rate.

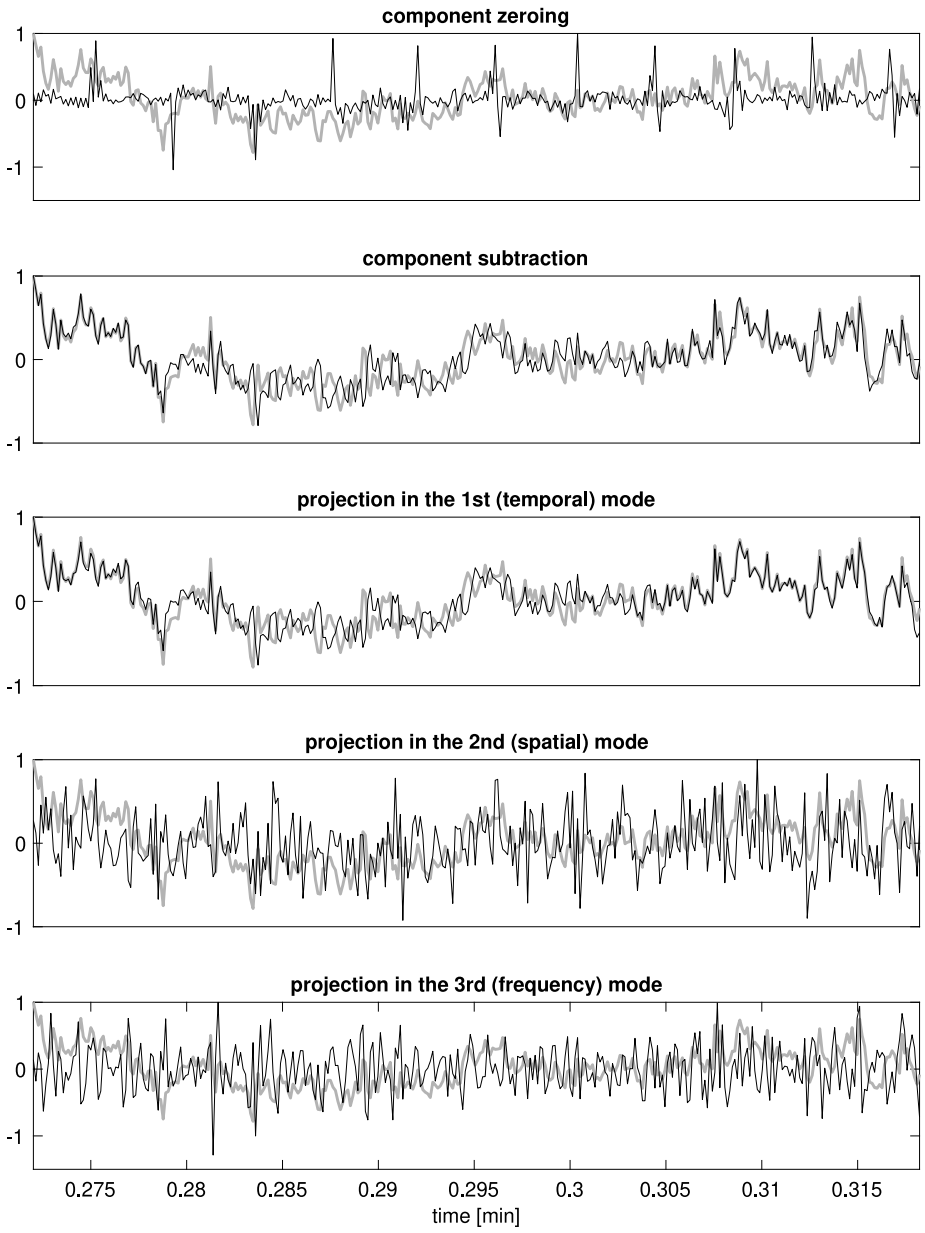

Fig. A.27. Sub1_med3: EEG signal from Fig. A.26 zoomed to a shorter time interval without any eye blink. The original (gray) and reconstructed signal (black) were normalized to unit maximal value to avoid visual discrepancies between them only due to multiplication.

B.1. CWT-Tuc-OC performance

In CWT-Tuc-OC, the data tensor has the size *number of time points* × *number of electrodes* × *number of CWT scales*. The tensor may be very large in the first mode depending on the measurement length and sampling rate. Using a standard computer (OS X, 3 GHz IntelCore i7 or M1 chip, 16 GB memory) and MATLAB [39], we were not able to run the Tucker model for EEG measurement exceeding 100 s (with 128 Hz sampling rate) due to memory overflow. Therefore, only results for the pre- and post-meditation data (SubX_pre, SubX_post) for all three subjects and Sub3_med data from Section 3 are included in this study.

In the first step, we analyzed the temporal, spatial, and scale signatures estimated by the Tucker model and their interpretation. Results for Sub1_pre are depicted in Fig. A.29. Despite the transformation of scales to pseudo-frequencies, the third mode or scale signatures (Fig. A.29, bottom right) are difficult to interpret, except for the first one. Regarding the spatial signatures (Fig. A.29, bottom left), the first signature SS 1, represents activity in the occipital region, typical for the occipital alpha rhythm, and SS 2 characterizes activity in the frontal region. The other spatial signatures are more difficult to interpret and are assumed to characterize noise. Nevertheless, Triantafyllopoulos and Megalooikonomou [24] analyzed only the first mode or temporal signatures in CWT-Tuc-OC, so we paid more attention to them.

In CWT-Tuc-OC, temporal signatures with absolute values of either normalized entropy or kurtosis exceeding 1.5 are selected as artifactual and set to zero vectors. Using this rule, we would choose TS 1, TS 8, and TS 10. However, looking at Fig. A.29 (top), we see that TS 2, TS 4, TS 6, TS 7, TS 11 or TS 12 have a similar profile to TS 1 and short intervals of their higher amplitude nicely overlap with the eye blink occurrence in the EEG signal from Fp1 electrode. Nevertheless, their absolute normalized entropy or kurtosis is under the threshold. On the other hand, TS 8 and TS 10 may represent some noise, but they do not follow the eye blink properties.

Therefore, we considered two versions for component selection: (i) normalized entropy or kurtosis exceeding 1.5, and (ii) visual criterion

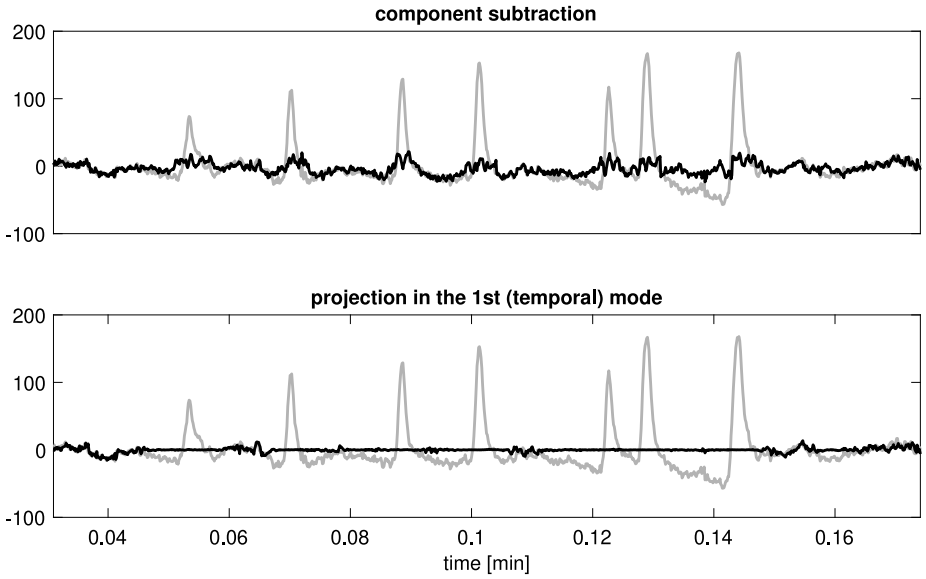

Fig. A.28. Sub1_med3: Comparison of the original, eye blink contaminated EEG signal (gray) from the Fp1 electrode and signal reconstructed by the SPECTER algorithm (black) on a short time interval with several eye blinks. In the SPECTER algorithm, the eye blink-related information was removed by (i) component subtraction and (ii) projection in the first (temporal) mode.

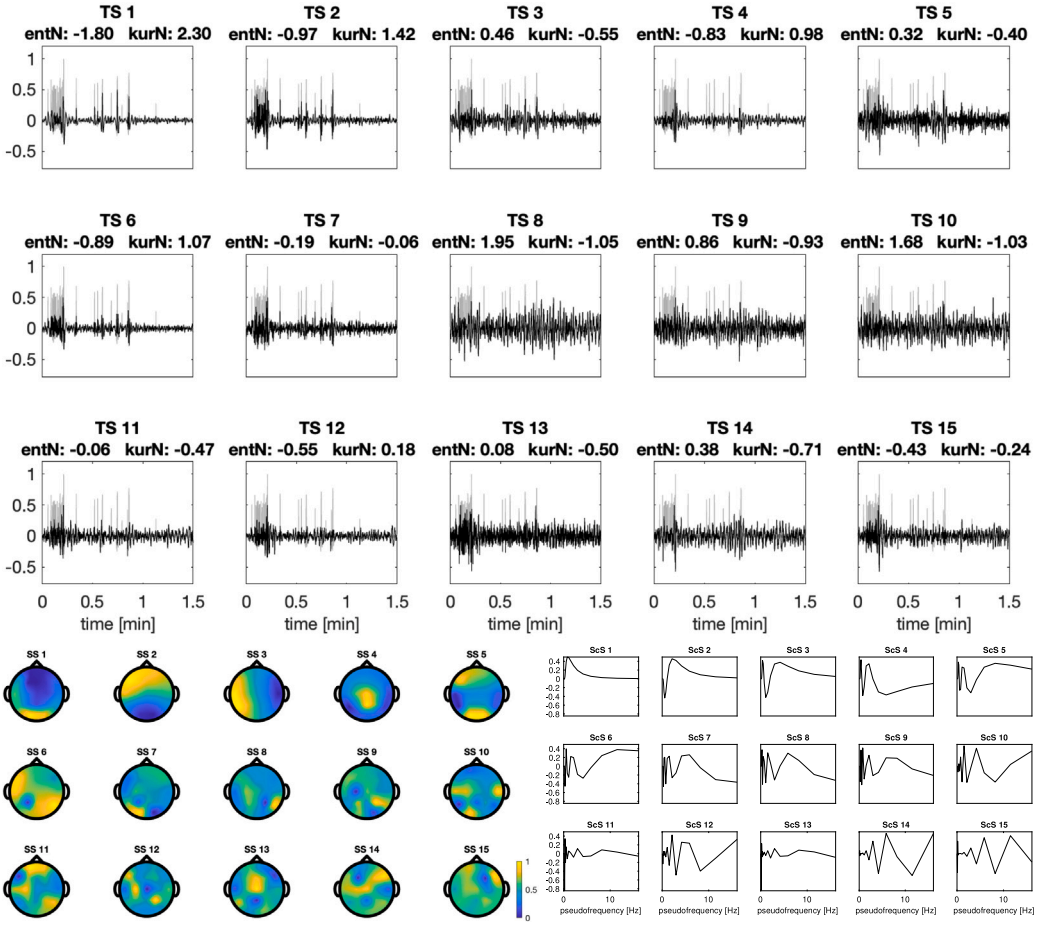

Fig. A.29. Sub1_pre: Temporal (TS, top), spatial (SS, bottom left), and scale (ScS, bottom right) signatures from the Tucker model with 15 components in each mode. Temporal signatures (black) are plotted with the rescaled EEG signal from the Fp1 electrode (gray). The normalized entropy (entN) and kurtosis (kurN) values are depicted in the titles of corresponding TS subfigures. To improve the interpretability of the third mode signatures, the CWT scales are transformed to pseudo-frequencies.

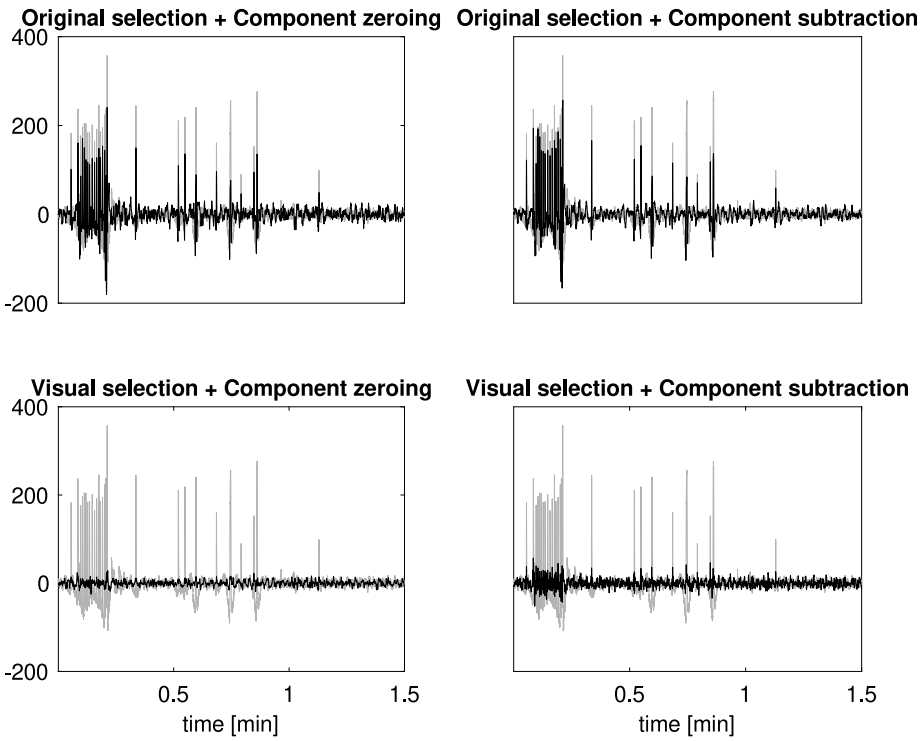

Fig. B.30. Sub1_pre: Original (gray) and reconstructed EEG signal from Fp1 electrode by CWT-Tuc-OC by using either original criterion for eye blink component selection (normalized entropy or kurtosis above 1.5), or visual inspection of temporal signatures. In addition to component zeroing, we considered component subtraction in the component removal step.

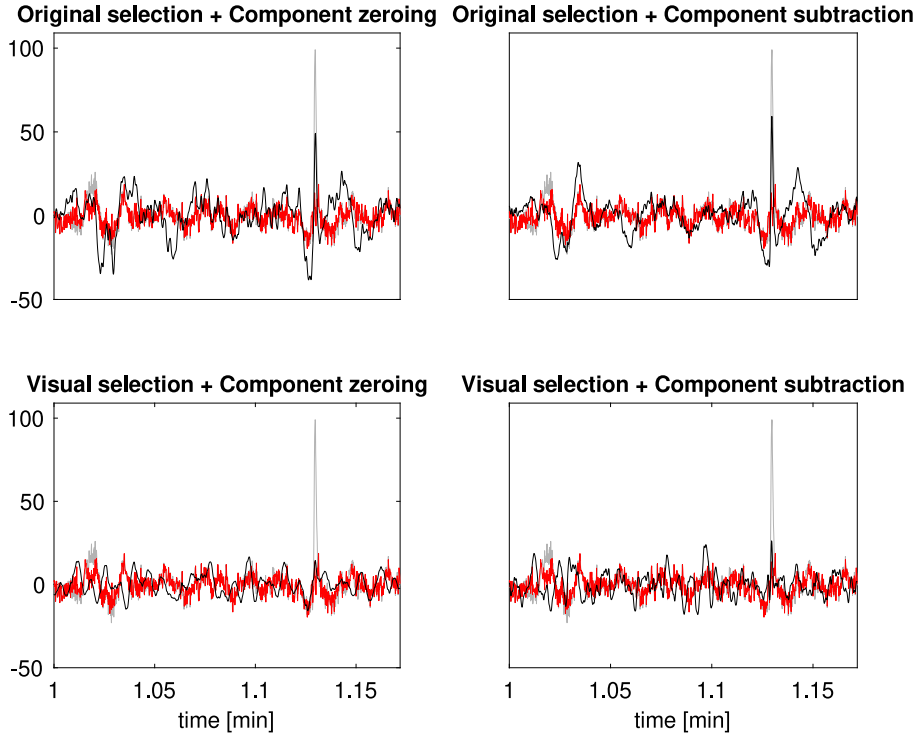

Fig. B.31. Sub1_pre: The same data from Fig. B.30 zoomed to a shorter time interval with one eye blink. The original EEG signal is in gray, the CWT-Tuc-OC reconstructed signal is in black, and the SPECTER result is in red.

based on the similarity between TS and EEG signal from the Fp1 electrode. The original CWT-Tuc-OC algorithm used component zeroing in the component removal step. However, due to inferior results produced by component zeroing and superior results provided by component subtraction in SPECTER, we also considered component subtraction in the CWT-Tuc-OC component removal step.

As depicted in Fig. B.30 (top), three components with normalized entropy or kurtosis over 1.5 removed either by component zeroing or component subtraction were not enough to properly remove eye blinks from Sub1_pre data. An improvement was observed when using subtraction of visually selected time signatures (Fig. B.30, bottom right), but several eye blinks, especially in the first third of measurement were still present. Visually the best results were obtained by visual selection of eye blink components in combination with component zeroing within CWT-Tuc-OC.

Nevertheless, we also inspected shorter intervals without or with one to two eye blinks where the differences between the original and CWT-Tuc-OC reconstructed signal became more visible. The results for Sub1_pre are depicted in Fig. B.31. Neither combination of component selection and component removal procedure in CWT-Tuc-OC produced satisfactory results. The reconstructed signal from the Fp1 electrode shows different behavior than the original EEG signal on non-blink intervals or in a neighborhood of a blink. On the other hand, the signal reconstructed by SPECTER visually overlaps with the original EEG signal (Fig. B.31, red).

Our attempts to improve the CWT-Tuc-OC results by selecting different combinations of time signatures with eye blink-related properties, applying constraints to the Tucker model, or using more scales in CWT did not lead to any improvement. Therefore, with the inability to process more extensive data, the CWT-Tuc-OC algorithm is not the best choice for eye blink removal in EEG signals.

References

[1] T. Elbert, W. Lutzenberger, B. Rockstroh, N. Birbaumer, Removal of ocular artifacts from the EEG - A biophysical approach to the EOG, Electroencephalogr. Clin. Neurophysiol. 60 (5) (1985) 455–463, http://dx.doi.org/10.1016/0013-4694(85)91020-X.

[2] G. Gratton, M.G. Coles, E. Donchin, A new method for off-line removal of ocular artifact, Electroencephalogr. Clin. Neurophysiol. 55 (4) (1983) 468–484, http://dx.doi.org/10.1016/0013-4694(83)90135-9.

[3] Y. Li, Z. Ma, W. Lu, Y. Li, Automatic removal of the eye blink artifact from EEG using an ICA-based template matching approach, Physiol. Meas. 27 (4) (2006) 425–436, http://dx.doi.org/10.1088/0967-3334/27/4/008.

[4] G.L. Wallstrom, R.E. Kass, A. Miller, J.F. Cohn, N.A. Fox, Automatic correction of ocular artifacts in the EEG: a comparison of regression-based and component-based methods, Int. J. Psychophysiol. 53 (2) (2004) 105–119, http://dx.doi.org/10.1016/j.ijpsycho.2004.03.007.

[5] C.A. Joyce, I.F. Gorodnitsky, M. Kutas, Automatic removal of eye movement and blink artifacts from EEG data using blind component separation, Psychophysiology 41 (2) (2004) 313–325, http://dx.doi.org/10.1111/j.1469-8986.2003.00141.x.

[6] T. Lagerlund, F. Sharbrough, N. Busacker, Spatial filtering of multichannel electroencephalographic recordings through principal component analysis by singular value decomposition, J. Clin. Neurophysiol.: Off. Publ. Am. Electroencephalogr. Soc. 14 (1) (1997) 73–82, http://dx.doi.org/10.1097/00004691-199701000-00007.

[7] O.G. Lins, T.W. Picton, P. Berg, M. Scherg, Ocular artifacts in EEG and event-related potentials I: Scalp topography, Brain Topogr. 6 (2005) 51–63.

[8] A. Hyvärinen, E. Oja, Independent component analysis: Algorithms and applications, Neural Netw. 13 (4–5) (2000) 411–430, http://dx.doi.org/10.1016/S0893-6080(00)00026-5.

[9] T.-P. Jung, S. Makeig, C. Humphries, T.-W. Lee, M.J. McKeown, V. Iragui, T.J. Sejnowski, Removing electroencephalographic artifacts by blind source separation, Psychophysiology 37 (2) (2000) 163–178, http://dx.doi.org/10.1111/1469-8986.3720163.

[10] M.B. Pontifex, V. Miskovic, S. Laszlo, Evaluating the efficacy of fully automated approaches for the selection of eyeblink ICA components, Psychophysiology 54 (5) (2017) 780–791.

[11] F. Miwakeichi, E. Martínez-Montes, P.A. Valdés-Sosa, N. Nishiyama, H. Mizuhara, Y. Yamaguchi, Decomposing EEG data into space–time–frequency components using Parallel Factor Analysis, NeuroImage 22 (3) (2004) 1035–1045, http://dx.doi.org/10.1016/j.neuroimage.2004.03.039.

[12] K. Nazarpour, S. Sanei, L. Shoker, J.A. Chambers, Parallel space-time-frequency decomposition of EEG signals for brain computer interfacing, in: 14th European Signal Processing Conference, IEEE, 2006, pp. 1–4.

[13] J. Dauwels, K. Srinivasan, R.M. Ramasubba, A. Cichocki, Multi-channel EEG compression based on matrix and tensor decompositions, in: 2011 IEEE International Conference on Acoustics, Speech and Signal Processing, ICASSP, 2011, pp. 629–632, http://dx.doi.org/10.1109/ICASSP.2011.5946482.

[14] M. Mørup, L.K. Hansen, C.S. Herrmann, J. Parnas, S.M. Arnfred, Parallel factor analysis as an exploratory tool for wavelet transformed event-related EEG, NeuroImage 29 (3) (2006) 938–947, http://dx.doi.org/10.1016/j.neuroimage.2005.08.005.

[15] F. Estienne, N. Matthijs, D. Massart, P. Ricoux, D. Leibovici, Multi-way modelling of high-dimensionality electroencephalographic data, Chemometr. Intell. Lab. Syst. 58 (1) (2001) 59–72, http://dx.doi.org/10.1016/S0169-7439(01)00140-X.

[16] R. Rosipal, N. Porubcová, P. Barančok, B. Cimrová, I. Farkaš, L.J. Trejo, Effects of mirror-box therapy on modulation of sensorimotor EEG oscillatory rhythms: a single-case longitudinal study, J. Neurophysiol. 121 (2) (2019) 620–633, http://dx.doi.org/10.1152/jn.00599.2018.

[17] Z. Rošťáková, R. Rosipal, S. Seifpour, L.J. Trejo, A comparison of non-negative Tucker decomposition and parallel factor analysis for identification and measurement of human EEG rhythms, Meas. Sci. Rev. 20 (3) (2020) 126–138, http://dx.doi.org/10.2478/msr-2020-0015.

[18] R.A. Harshman, Foundations of the PARAFAC Procedure: Models and Conditions for an "Explanatory" Multimodal Factor Analysis, UCLA Working Papers in Phonetics 16, University of California at Los Angeles, Los Angeles, CA, 1970, pp. 1–84.

[19] J.D. Carroll, J.-J. Chang, Analysis of individual differences in multidimensional scaling via an N-way generalization of "Eckart-Young" decomposition, Psychometrika 35 (3) (1970) 283–319, http://dx.doi.org/10.1007/BF02310791.

[20] L.R. Tucker, Some mathematical notes on three-mode factor analysis, Psychometrika 31 (3) (1966) 279–311, http://dx.doi.org/10.1007/BF02289464.

[21] R. Rosipal, Z. Rošťáková, L.J. Trejo, Tensor decomposition of human narrowband oscillatory brain activity in frequency, space and time, Biol. Psychol. 169 (2022) 108287, http://dx.doi.org/10.1016/j.biopsycho.2022.108287.

[22] E. Acar, C. Aykut-Bingol, H. Bingol, R. Bro, B. Yener, Multiway analysis of epilepsy tensors, Bioinformatics 23 (13) (2007) 10–18, http://dx.doi.org/10.1093/bioinformatics/btm210.

[23] K. Nazarpour, H. Mohseni, C. Hesse, J. Chambers, S. Saied, A novel semiblind signal extraction approach for the removal of eye-blink artifact from EEGs, EURASIP J. Adv. Signal Process. 2008 (2008) http://dx.doi.org/10.1155/2008/857459.

[24] D. Triantafyllopoulos, V. Megalooikonomou, Eye blink artifact removal in EEG using tensor decomposition, in: IFIP International Conference on Artificial Intelligence Applications and Innovations, Springer, 2014, pp. 155–164, http://dx.doi.org/10.1007/978-3-662-44722-2_17.

[25] Y. Masuyama, K. Yatabe, Y. Oikawa, Griffin-Lim like phase recovery via alternating direction method of multipliers, IEEE Signal Process. Lett. PP (2018) 1, http://dx.doi.org/10.1109/LSP.2018.2884026.

[26] A. Cichocki, R. Zdunek, A.H. Phan, S. Amari, Nonnegative matrix and tensor factorizations: applications to exploratory multi-way data analysis and blind source separation, John Wiley & Sons, United Kingdom, 2009.

[27] R. Bro, N.D. Sidiropoulos, Least squares algorithms under unimodality and non-negativity constraints, J. Chemometr. 12 (4) (1998) 223–247, http://dx.doi.org/10.1002/(SICI)1099-128X(199807/08)12:4<223::AID-CEM511>3.0.CO;2-2.

[28] D. Griffin, J. Lim, Signal estimation from modified short-time Fourier transform, IEEE Trans. Acoust. Speech Signal Process. 32 (2) (1984) 236–243, http://dx.doi.org/10.1109/TASSP.1984.1164317.

[29] N. Perraudin, P. Balazs, P. Søndergaard, A fast Griffin-Lim algorithm, in: IEEE Workshop on Applications of Signal Processing to Audio and Acoustics, 2013, pp. 1–4, http://dx.doi.org/10.1109/WASPAA.2013.6701851.

[30] X. Zhu, G. Beauregard, L. Wyse, Real-time signal estimation from modified short-time Fourier transform magnitude spectra, IEEE Trans. Audio Speech Lang. Process. 15 (2007) 1645–1653, http://dx.doi.org/10.1109/TASL.2007.899236.

[31] Z. Průša, P. Balazs, P.L. Søndergaard, A noniterative method for reconstruction of phase from STFT magnitude, IEEE/ACM Trans. Audio Speech Lang. Proc. 25 (5) (2017) 1154–1164, http://dx.doi.org/10.1109/TASLP.2017.2678166.

[32] R. Bro, PARAFAC. Tutorial and applications, Chemometr. Intell. Lab. Syst. 38 (2) (1997) 149–171, http://dx.doi.org/10.1016/S0169-7439(97)00032-4.

[33] Z. Rošťáková, R. Rosipal, Determination of the number of components in the PARAFAC model with a nonnegative tensor structure: a simulated EEG data study, Neural Comput. Appl. (2022) http://dx.doi.org/10.1007/s00521-022-07318-x.

[34] M. Ester, H.-P. Kriegel, J. Sander, X. Xu, A density-based algorithm for discovering clusters in large spatial databases with noise, in: Second International Conference on Knowledge Discovery & Data Mining, AAAI Press, USA, 1996, pp. 226–231.

[35] A. Mognon, J. Jovicich, L. Bruzzone, M. Buiatti, ADJUST: An automatic EEG artifact detector based on the joint use of spatial and temporal features, Psychophysiology 48 (2) (2011) 229–240, http://dx.doi.org/10.1111/j.1469-8986.2010.01061.x.

[36] A. Delorme, S. Makeig, EEGLAB: an open source toolbox for analysis of single-trial EEG dynamics including independent component analysis, J. Neurosci. Methods 134 (1) (2004) 9–21, http://dx.doi.org/10.1016/j.jneumeth.2003.10.009.

[37] R. Mahajan, B. Morshed, Unsupervised eye blink artifact denoising of EEG data with modified multiscale sample Entropy, Kurtosis, and Wavelet-ICA, IEEE J. Biomed. Health Inform. 19 (2014) http://dx.doi.org/10.1109/JBHI.2014.2333010.

[38] M. Müller, Dynamic time warping, Inf. Retr. Music Motion (2007) 69–84.

[39] The Mathworks, Inc, MATLAB Version 9.10.0.1684407 (R2021a), Natick, Massachusetts, 2021.

[40] J.M.A. Tanskanen, F.E. Kapucu, I. Vornanen, J.A.K. Hyttinen, Automatic objective thresholding to detect neuronal action potentials, in: 2016 24th European Signal Processing Conference, EUSIPCO, 2016, pp. 662–666, http://dx.doi.org/10.1109/EUSIPCO.2016.7760331.

[41] L.J. Trejo, R. Rosipal, P.L. Nunez, Advanced Physiological Estimation of Cognitive Status (APECS), Final project report, Tech. rep., Research Triangle Park, NC: U.S. Army Research Office, 2009, URL https://apps.dtic.mil/sti/pdfs/ADA520986.pdf.

[42] Brain Products, GmbH, BrainVision Analyser 2, 2013.

[43] M. Plank, Ocular Correction ICA, 2022, URL https://www.brainproducts.com/support-resources/ocular-correction-ica/#:~:text=Taken. (Accessed 10 August 2023).

[44] R. Kobler, A.-I. Sburlea, G. Müller-Putz, A comparison of ocular artifact removal methods for block design based electroencephalography experiments, in: Proceedings of the 7th Graz Brain-Computer Interface Conference 2017, 2017, pp. 236–241, http://dx.doi.org/10.3217/978-3-85125-533-1-44.

[45] R. Kobler, A.-I. Sburlea, G. Müller-Putz, Tuning characteristics of low-frequency EEG to positions and velocities in visuomotor and oculomotor tracking tasks, Sci. Rep. 8 (2018) 17713, http://dx.doi.org/10.1038/s41598-018-36326-y.

[46] V. Mondini, R. Kobler, A.-I. Sburlea, G. Müller-Putz, Continuous low-frequency EEG decoding of arm movement for closed-loop, natural control of a robotic arm, J. Neural Eng. 17 (2020) 046031, http://dx.doi.org/10.1088/1741-2552/aba6f7.

[47] C. Lopes-Dias, A.-I. Sburlea, G. Müller-Putz, Online asynchronous decoding of error-related potentials during the continuous control of a robot, Sci. Rep. 17596 (2019) http://dx.doi.org/10.1038/s41598-019-54109-x.

[48] A. Schwarz, J. Pereira, R. Kobler, G. Müller-Putz, Unimanual and bimanual reach-and-grasp actions can be decoded from human EEG, IEEE Trans. Biomed. Eng. (2019) 1684–1695, http://dx.doi.org/10.1109/TBME.2019.2942974.

[49] M.A. Klados, C. Papadelis, C. Braun, P.D. Bamidis, REG-ICA: A hybrid methodology combining blind source separation and regression techniques for the rejection of ocular artifacts, Biomed. Signal Process. Control 6 (3) (2011) 291–300, http://dx.doi.org/10.1016/j.bspc.2011.02.001, ITAB 2009.

[50] R. Patel, K. Gireesan, S. Sengottuvel, Decoding non-linearity for effective extraction of the eye-blink artifact pattern from EEG recordings, Pattern Recognit. Lett. 139 (2020) 42–49, http://dx.doi.org/10.1016/j.patrec.2018.01.022.

[51] B.W. Bader, T.G. Kolda, Tensor toolbox for MATLAB, version 3.2.1, 2021, www.tensortoolbox.org.